Chem Biol Drug Des 2009; **74:** 101–120

Review Article

© 2009 John Wiley & Sons A/S

doi: 10.1111/j.1747-0285.2009.00847.x

Circular Dichroism Techniques: Biomolecular and Nanostructural Analyses- A Review

Bijan Ranjbar[1,2,*] and Pooria Gill[2]

[1]*Department of Biophysics, Faculty of Biological Sciences, Tarbiat Modares University, Tehran, Iran*

[2]*Department of Nanobiotechnology, Faculty of Biological Sciences, Tarbiat Modares University, Tehran, Iran*

**Corresponding author: Bijan Ranjbar, ranjbarb@modares.ac.ir*

This paper reviews the best known techniques using circular dichroism spectroscopy such as conventional circular dichroism (i.e. electronic circular dichroism), magnetic circular dichroisms (magnetic vibrational circular dichroism, x-ray magnetic circular dichroism), fluorescence detected circular dichroism, near-infrared circular dichroism, vibrational circular dichroism, Fourier transform infrared circular dichroism, high pressure liquid chromatography circular dichroism, stopped-flow circular dichroism, and synchrotron radiation circular dichroism. Also, we have described here the most important applications of circular dichroism spectroscopy in structural biochemistry and nanoscience.

Key words: biomolecular analysis, chirality, circular dichroism, FDCD, FTIR-VCD, HPLC-CD, MCD, MVCD, nanostructural analysis, NIR-CD, SRCD, stopped-flow CD, VCD, XMCD

Abbreviations: A, adenosine; AC, absolute configuration; AIDS, acquired immunodeficiency syndrome; ApA, adenylyl-3′-5′-adenosine; BAA, *Bacillus amyloliquefaciens* α-amylase; BSA, bovine serum albumin; CD, circular dichroism; CPP, cell penetrating peptide; Den, dendrosome; DFT, density functional theory; DMPC, dimyristoylphosphatidylcholine; DNA, deoxyribonucleic acid; DPC, dodecylphosphocholine; DPPC, dipalmitoylphosphatidylcholine; DTT, dithiothreitol; ECD, electronic circular dichroism; EDTA, ethylene diamino tetra acetic acid; FDCD, fluorescence detected circular dichroism; FE, Faraday effect; FNG, fibrinogen; FTIR, Fourier transform infrared; Hb, haemoglobin; HPLC, high pressure liquid chromatography; IR, infrared; LCP, left circularly polarized light; LUV, large unilamellar vesicles; M, mutant; MCD, magnetic circular dichroism; MVCD, magnetic vibrational; N, native; NIR, near-infrared; NP, nanoparticle; PBzE dendrimer, poly(benzyl ether) dendrimer; PC liposomes, phosphatidylcholine liposomes; PDT, photodynamic therapy; PEHA, poly(2-ethylhexylacrylate); PEM, photo elastic modulator; PHEMA, poly(2-hydroxyethyl methacrylate); PMEA, poly (2-methoxyethylacrylate); PNA, peptide nucleic acids; PPII, polyproline II; Pro, proline; RCP, right circularly polarized; rLuc, recombinant luciferase; RNA, ribonucleic acid; SAP, sweet arrow peptide; SDS, micelles, sodium dodecyl sulphate micelles; SRCD, synchrotron radiation circular dichroism; UV, ultraviolet; VCD, vibrational circular dichroism; vis, visible; VUV, vacuum-ultraviolet; XMCD, x-ray magnetic circular dichroism; ZE, Zeeman effect; θ, dihedral angle.

Received 25 January 2009, revised 4 May 2009 and accepted for publication 16 May 2009

Some biomolecules possess molecular asymmetry, that is, their mirror images are not identical. Such molecules are named to be chiral (1). One of the most well-known examples is a carbon atom that is tetrahedrally bonded to four different atoms or groups of atoms. Biomacromolecules also show chirality. For example, the α-helix, the most common helix in proteins, is wound in a right--hand sense. Although most polynucleotides are wound in a right-hand sense, helices that wind in a left hand sense also exist (2).

The interaction of a chiral molecule with polarized light (Figure 1) is very specific and has proved to be an important method for characterizing both small molecule and macromolecular structures (3). Essentially, one type of measurements commonly made to determine the effects of polarized light on asymmetric molecules is circular dichroism (CD) (1), which is defined as the difference in absorption of left-hand and right-hand circularly polarized light with optically active compounds.

These effects are relatively small but can be measured readily with modern instrumentation. Hence, measurement of circular dichroism gives detailed structural and enantiomeric information on proteins, carbohydrates, nucleic acids, pharmaceuticals, liquid crystals, etc. (3). For example, the conversion of simple peptides into the destructive fibrils in some disorders such as Alzheimer disease can be followed using CD (4,5).

In last decades, there have been encountered various developments in CD-based techniques to improve the molecular measurements of biological structures (6). The best known of them are conventional CD/electronic circular dichroism (ECD), magnetic CDs (MCD, magnetic vibrational circular dichroism (MVCD), XMCD), fluorescence detected CD (FDCD), near-infrared CD (NIR-CD), vibrational CDs (VCD, FTIR-VCD), HPLC-CD, stopped-flow CD, and synchrotron radiation CD (SRCD). In this review, various kinds of CD-spectroscopy techniques and their applications in biological studies and nanostructural analyses have been discussed.

Circular Dichroism

Description

Dichroism is often expressed as the property possessed by some materials of absorbing light to different extents dependent upon

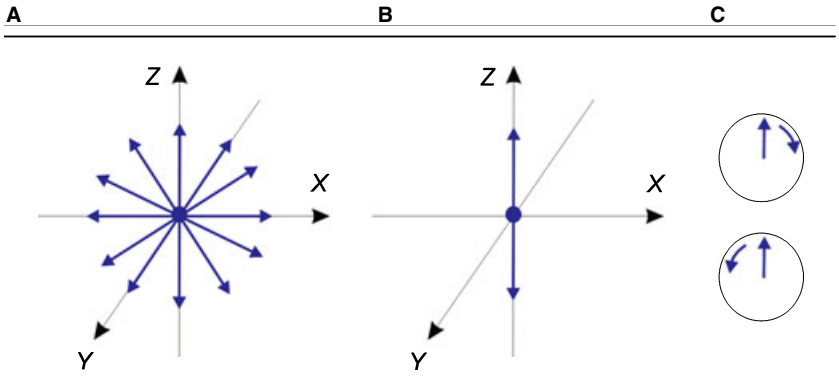

Figure 1: Schemes of the electric field components of unpolarized (A), linearly or plane polarized light (B). The light is moving along the *y*-axis. For unpolarized light, all directions occur, whereas for linearly or plane polarized light only the *z*-direction is found. For circularly polarized light (C), the direction of rotation can be clockwise or counterclockwise.

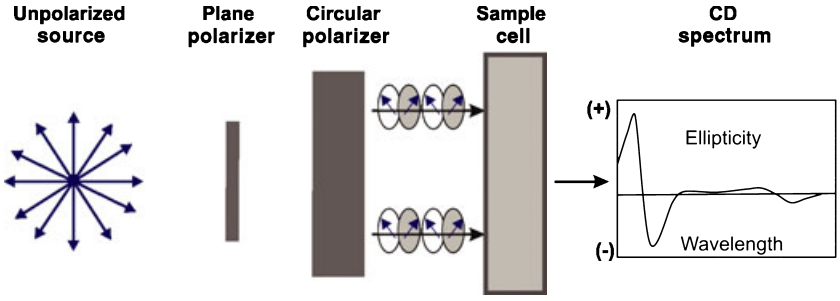

Figure 2: Scheme of CD in which a difference in absorption is measured.

the polarization form of the incident beam. Where the absorption of light circularly polarized in one direction (right-handed) is different from the absorption of the light circularly polarized in the opposite direction (left handed), the material is said to exhibit circular dichroism (Figure 2) (1,2,7–9).

When the light is circularly polarized, a secondary absorbance component arises from circular dichroism. The secondary absorbance component is measured by switching between left and right circularly polarized (RCP) light, and measuring the resulting difference in absorbance (2,7).

Any conformational changes in the structure of macromolecules could be assessed using circular dichroism. As a consequent, unfolding of biomolecules (such as proteins, nucleic acids, glycosides, etc.) is measured as a change in circular dichroism (CD) spectra, and serves to give a measure of the relative quantities of changes have been made in the components. As for absorption spectra, as is known in the art for example, native proteins have a characteristic CD spectra, with small changes unique to each particular protein (3,9). The shape of the spectra curve, as well as the positive maxima and negative maxima, provide information about the protein. Thus, for example, peaks present in the 200–250 nm wavelength ('far-UV') range are generally a 'w'-shaped spectra with troughs around 222 and 208 being indicative of the presence of α-helical structures, and a 'v'-shaped spectra with a trough around 21 7–220 nm being indicative of β-sheet structures. However, the accuracies have been reported for CD are 97% for helices, 75% for beta sheet, 50% for turns, and 89% for other secondary structures, respectively (10). Scans in the 'near-UV' range, i.e. 250–300 nm, give information about tertiary structure. Other parts of the spectrum, as around 410 nm for haeme proteins, may yield structural information as well (11).

The main unit has been defined for circular dichroism is 'ellipticity', which is described as the tangent of the ratio of the minor to major elliptical axis. In the other word, the occurrence of ellipticity is called circular dichroism (1). According to the literature, for reporting the CD of a sample, mean residue ellipticity (degree cm^2 $dmol^{-1}$) and molar circular dichroism or delta epsilon (L mol^{-1} cm^{-1}) are common (2).

As we describe in the following modes, applications of CD spectroscopy could be categorized in various regions of biological studies such as: (i) conformational assessments of proteins and nucleic acids; (ii) determination of the thermodynamics of folding and unfolding of biomolecules; (iii) interactional studies of asymmetric biomolecules (e.g. protein–protein interactions, protein–DNA interactions, protein–ligand interactions, and DNA–ligand interactions); and (iv) kinetics of folding and unfolding of macromolecules.

Protein analyses

Determination of protein secondary structure

Protein secondary structure can be determined by CD spectroscopy in the 'far-UV' spectral region (190–250 nm). At these wavelengths, the chromophore is the peptide bond, and the signal arises when it is located in a regular, folded environment (11). The weakest energy transition in the peptide chromophore is an $n \rightarrow \pi^*$ transition observed at 210–220 nm, which involves non-bonding electrons of

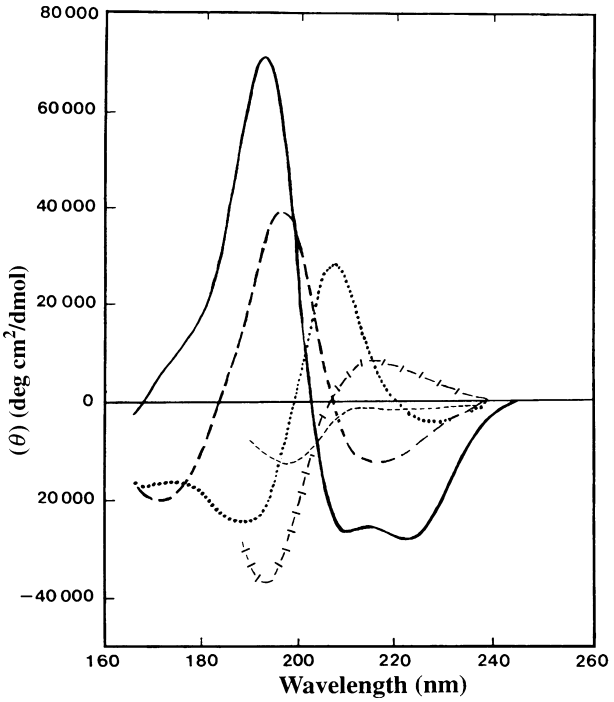

Figure 3: Illustration of graphs showing far-UV CD spectra associated with various types of secondary structure. Solid line, α-helix; long dashed line, antiparallel β-sheet; dotted line, type I β-turn; cross-dashed line, extended 3_1-helix or poly (Pro) II helix; short-dashed line, irregular structure. The data are adapted from Kelly *et al.* (12).

O of the carbonyl. However, the strongest energy one is an absorption band centred at 190 nm because of $\pi \rightarrow \pi^*$ transition involved the π-electrons of the carbonyl (1,2). Hence, the intensity of the transitions depends on Φ and Ψ torsion angles. The α-helix, β-sheet, and random coil structures each give rise to a characteristic shape and magnitude of CD spectrum (Figure 3) (12).

For revealing any secondary structure in proteins, there are particular characteristics for CD spectra. As determined, far-UV-CD of random coil is positive at 212 nm ($n \rightarrow \pi^*$) and negative at 195 nm ($\pi \rightarrow \pi^*$). Far-UV-CD of β-sheet is negative at 218 nm ($\pi \rightarrow \pi^*$) and positive at 196 nm ($n \rightarrow \pi^*$). For α-helix, the exciton coupling of the $\pi \rightarrow \pi^*$ transitions leads to positive ($\pi \rightarrow \pi^*$) perpendicular at 192 nm, negative ($\pi \rightarrow \pi^*$) parallel at 208 nm, and negative at 222 nm is red shifted ($n \rightarrow \pi^*$), respectively (10,12). The approximate fraction of each secondary structure type that is present in any protein can thus be determined by analysing its far-UV CD spectrum as a sum of fractional multiples of such reference spectra for each structural type. Although CD spectra reflect an average of the whole molecules (e.g. 50% of a protein contains beta-sheet), the technique is not powerful to determine which specific residues are participated in the portion (2,12).

Technically, far-UV CD spectra require 20–200 μL of solution containing 1 mg/mL to 50 μg/mL protein, in any buffer which does not have a high absorbance in this region of the spectrum (such as

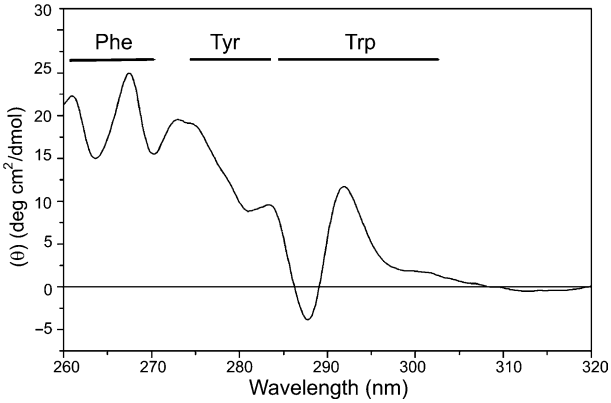

Figure 4: The near-UV Circular dichroism spectrum for type II dehydroquinase from *Streptomyces coelicolor.* The wavelength ranges corresponding to signals from Phe, Tyr and Trp side chains are indicated. The data are adapted from Kelly *et al.* (12) and Krell *et al.* (14).

high concentrations of dithiothreitol, histidine, or imidazole, for example, cannot be used in the far-UV region) (12,13).

Information about protein tertiary structure

The CD spectrum of a protein in the 'near-UV' spectral region (250–320 nm) can be sensitive to certain aspects of tertiary structure (Figure 4). At these wavelengths, the chromophores are the aromatic amino acids and disulfide bonds, and the CD signals they produce are sensitive to the overall tertiary structure of the protein (12).

Aromatics have allowed $\pi \rightarrow \pi^*$ transitions that are directed in the plane of the π-bonding system and are orthogonal to each other (13). Signals in the region from 255–270 nm are attributable to phenyl group of phenylalanine residues, whereas signals from 275–285 nm are attributable to phenolic group of tyrosine, and those from 285–305 nm are attributable to indole group of tryptophan. Disulfide bonds give rise to broad weak signals throughout the near-UV spectrum with no vibronic structure (12–15).

The near-UV CD spectrum can be sensitive to small changes in tertiary structure due to protein–protein interactions and/or changes in solvent conditions (15). The signal strength in the near-UV CD region is much weaker than that in the far-UV CD region. Near-UV CD spectra require about 1 mL of protein solution with an optical density at 280 nm of 0.5–1 (which corresponds to 0.5 to 1 mg/mL for most proteins) (13–15).

Demonstrating comparability of conformation

Often it is necessary to demonstrate that a modification on a protein have equivalent conformations (Figure 5) to do its function properly. For example, after a modification (chemically/genetically) on specific protein, CD can be a good technique for comparison between native and modified forms (16–18).

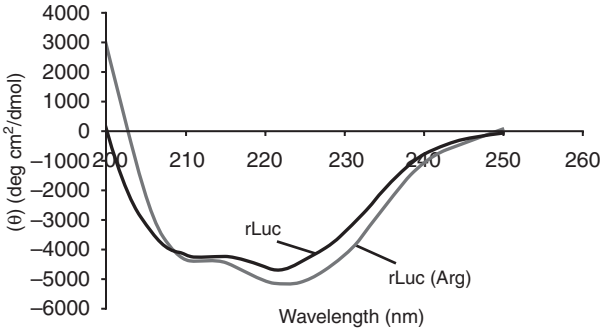

Figure 5: Far-UV CD spectra for native luciferase (rLuc) and mutant luciferase (rLuc (Arg)). The data are adapted from Kh. Tafreshi *et al.* (16).

For instance, it was indicated that the expression of an active mutant luciferase (rLuc (Arg)) under the same condition as the native form (rLuc) suggests formation and refolding of a properly folded luciferase without aggregation, which has been confirmed by CD (Figure 5) (16).

Thermal stability

Thermal stability is assessed using CD by following changes in the spectrum with increasing temperature (Figure 6) (11). In some cases, the entire spectrum in the far- or near-UV CD region can be followed at a number of temperatures. Alternatively, a single wavelength can be chosen which monitors some specific feature of the protein structure, and the signal at that wavelength is then recorded continuously as the temperature is raised. CD is often used to assess the degree to which solution pH, buffers, and additives such as sugars, amino acids or salts alter the thermal stability (19,20).

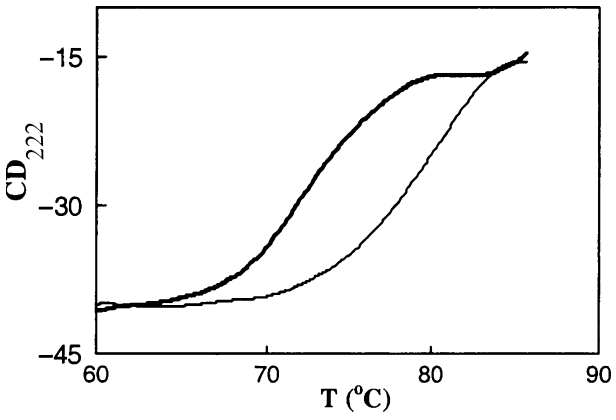

Figure 6: Schematic illustration of thermal scans done for the same protein (BAA) in two different buffers. CD at 222 nm exhibited by BAA at various temperatures in Tris buffer in (thick line) absence and (thin line) presence of 10 mM $CaCl_2$. In the absence and presence of Ca^{2+}, the Tm values of BAA were 71.7 and 80 °C, respectively. Data are adapted from Hassan Sajedi *et al.* (19).

Many proteins aggregate or precipitate quickly after they are unfolded ('melted'), making unfolding irreversible. The reversibility of the unfolding reaction can be assessed by cooling the sample and then heating again to see if the unfolding reaction is duplicated (11). Finding solvent conditions that make unfolding reversible may be actually more important for long-term stability (shelf-life) than raising the melting temperature. If the melting is fully reversible, the melting temperature is directly related to conformational stability, and the thermodynamics of protein folding can be extracted from the CD data (12). If the protein precipitates or aggregates as it is unfolded, the melting reaction will be irreversible, and the melting temperature will reflect the kinetics of aggregation and the solubility of the unfolded form of the molecule as well as the intrinsic conformational stability. The cooperativity of the unfolding reaction is measured qualitatively by the width and shape of the unfolding transition (13). A highly cooperative unfolding reaction indicates that the protein existed initially as a compact, well-folded structure, while a very gradual, non-cooperative melting reaction indicates that the protein existed initially as a very flexible, partially unfolded protein or as a heterogeneous population of folded structures (11,12).

Melting of secondary structure By following changes over the entire far-UV CD region, it can be determined whether at high temperatures the protein is losing all of its secondary structure, loses only a portion of its secondary structure, or simply undergoes conformational change involving a change in secondary structure (Figure 7) (21,22). Occasionally, the unfolded form of a protein will possess a defined, but totally different secondary structure than the native form (12,13).

Melting of tertiary structure Changes in tertiary structure can be followed by monitoring changes in the near-UV CD region. Such studies will reveal whether the melting of a protein occurs in a

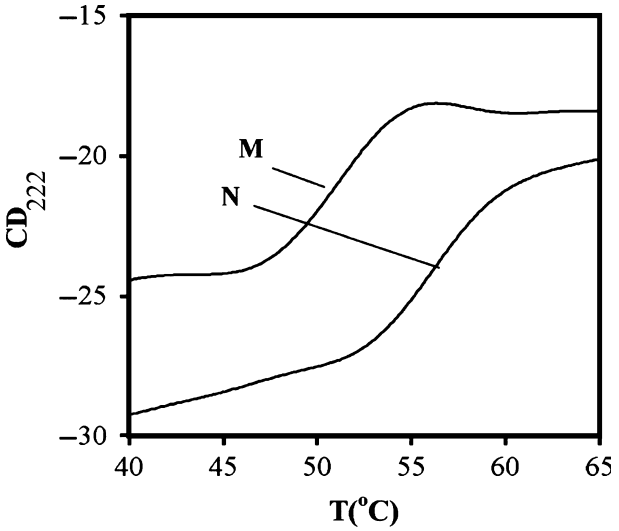

Figure 7: Melting profiles of native (N) and mutant (M) luciferase. Spectra were taken at 25–70 °C by far-UV CD in phosphate buffer (0.95 M, pH 7.0). Data are adapted from Riahi Madvar *et al.* (21).

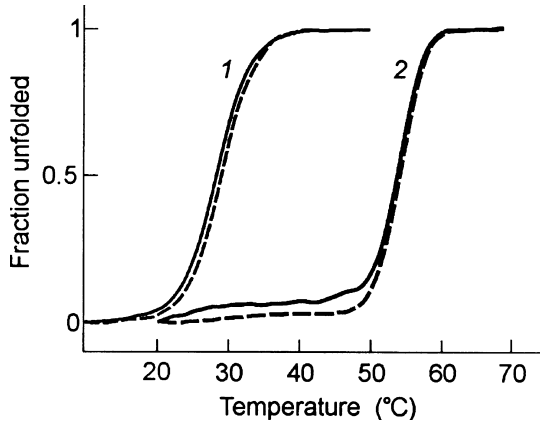

Figure 8: Melting curves for barnase at (1) pH 2.4 and (2) pH 5.5 from the temperature dependence of CD at 280 (solid line) and 194 nm (dashed line). Data are adapted from Schulga *et al*. (23).

single-step reaction (with concurrent loss of both secondary and tertiary structure), or in a two-step reaction (13,15).

For instance, melting curves for barnase as the CD versus temperature in the far-(194 nm) and near-UV (280 nm) at pH 5.5 and 2.4 (Figure 8) indicated the steep decrease in CD at 194 nm with rising temperature is due to cooperative melting of secondary structure, and the decrease in CD at 280 nm indicated loss of tertiary structure. The congruence of the 194 and 280 nm melting curves confirmed that the alterations in secondary and tertiary structures are concurrent (23).

Melting of protein complexes The effect of forming a protein–protein complex (e.g. ligand/receptor, antigen–antibody, or dimers/polymers) on the thermal stability of the individual proteins in the complex can also be determined (Figure 9) (24). This works best if the individual proteins have CD spectra which are quite different from each other, such that changes at specific wavelengths can be monitored to follow changes in the corresponding protein. In such cases, it is possible to determine whether there is an increase in stability of one or both of the proteins following complex formation (25).

The thermal unfolding of monomer and dimer of lysozyme at pH 2 (Figure 9) indicated the monomer transition was sigmoidal with a midpoint Tm (about 52 °C), but in the dimer form the thermal unfolding was not sigmoidal, and its stability has been changed (24).

Detection of molten globule-like structure of proteins

Molten globule is a stable, partially folded protein state found in mildly denaturing conditions such as low pH, mild denaturant or high temperature (26). Molten globules are collapsed and generally have some native-like secondary structure but a dynamic tertiary structure as seen by far and near circular dichroism spectroscopy, respectively (27–31). These traits are similar to those observed in

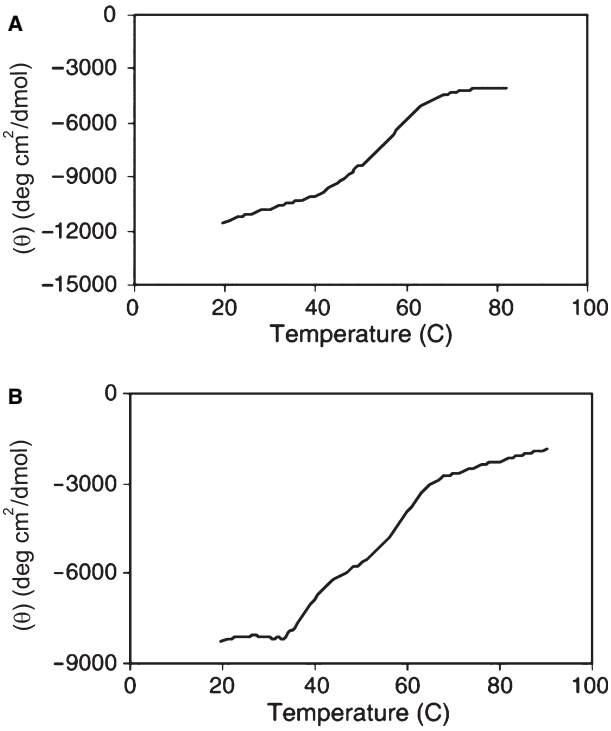

Figure 9: Thermal unfolding of lysozyme monomer (A), and lysozyme dimer (B) as a complex protein at pH 2 monitored at 222 nm. Data are adapted from Maroufi *et al*. (24).

the transient intermediate states found during the folding of certain proteins, especially globular proteins that undergo hydrophobic collapse, and therefore the term 'molten globule' is also used to refer to certain protein folding intermediates corresponding to the narrowing region of the folding funnel higher in energy than the native state but lower than the denatured state. The molten globule ensembles sampled during protein folding and unfolding are thought to be roughly similar (32).

The experimental studies of the folding intermediates of various globular proteins have demonstrated that the molten globule is a real productive intermediate of folding (33). The structural characteristics of the molten globule state are apparent and common among different proteins, and indicate that the state is structurally intermediate between the native and the fully unfolded state (34).

Comparisons between the CD spectra in near-UV and Far-UV regions of a protein could clarify how modifications affected its structure (Figure 10). For example, the transition to the molten globule state has been shown to be accompanied by loss of tertiary interactions whereas most of the secondary structure is preserved. This is manifested by the disappearance of the CD bands in the near-UV region and the virtually unchanged CD spectrum in the far-UV region (31,35,36). As a consequent, if a protein retains secondary structure but no defined three-dimensional structure (e.g. an incorrectly folded or 'molten-globule' structure), the signals in the near-UV region will be nearly zero (31). On the other hand, the presence of

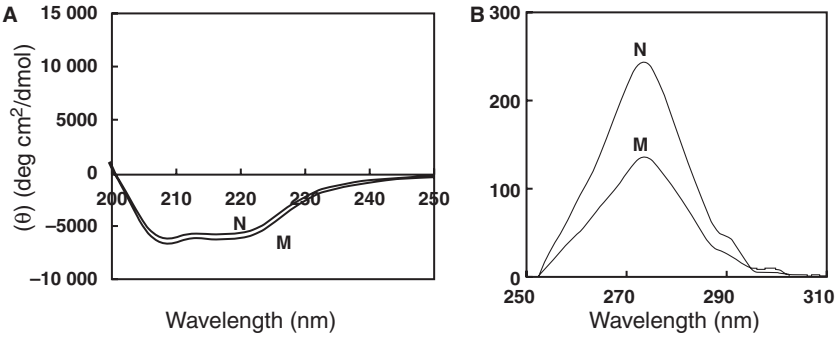

Figure 10: Far-UV CD spectra (A) and near-UV CD spectra (B) for native (N) and modified (M) glucose oxidase. Data are adapted from Hosseinkhani *et al.* (31).

significant near-UV signals is a good indication that the protein is folded into a well-defined structure.

Biophysical analyses of cell-penetrating peptides

Cell penetrating peptides (CPPs) are peptides with the capacity to translocate across the plasma membrane of mammalian cells (37). These biological macromolecules, have created a new horizon in biomedical research to obtain most efficient ways to carry substantial cargoes such as peptides (38,39), proteins (40), plasmid DNA (41), oligonucleotides (42), peptide nucleic acids (PNA) (43,44), and even nanoparticles (45) or liposomes (46) across the plasma membrane into cellular compartments. Circular dichroism allows a quick estimation of secondary structures of cell-penetrating peptides and is well suited for following changes in their secondary structures dependent on peptide concentration, pH, buffer, and on the nature and composition of the lipid (47).

For instance, the presence of the polyproline II (PPII) secondary structure in a Pro-rich peptide (as a CPP) can be easily assessed by circular dichroism (48,49). The PPII spectrum presents a weak positive band at 228 nm and a strong negative band at 203 nm. Because of the weakness of the positive band, it is only observed when working at low temperatures (Figure 11, inset). When rising the temperature, the peptide PPII structure becomes more flexible, causing a decrease in the intensity of both bands (Figure 11) (48).

Similarly, the secondary structure of penetratin (as a CPP) has been determined in a number of studies under various conditions. As a general trend, penetratin is mainly unstructured in buffer (occasionally with a significant β-sheet contribution) and becomes α-helical in SDS micelles and neutral PC liposomes, whereas negatively charged liposomes induced β-sheet formation (50–53). In another study (54), it was demonstrated that the α-helix to β-sheet transition occurred during vesicle aggregation and a subsequent transformation back to an α-helical conformation took place during the spontaneous disaggregation. Sequence modifications of penetratin in which one or two Trp were replaced by Phe had a propensity to adopt the β-sheet structure, while penetratin without this modification had a propensity for the α-helical form (53). In general, the secondary structure of penetratin appears to be highly dependent on various key factors, like type and charge of lipid, concentration, and peptide-to-lipid ratio. In contrast to penetratin, CD analyses shown that the secondary structure of transportan was less variable and independent of lipid charge density. Transportan displayed about 30% α-helicity in water and 50–60% in membrane model systems like SDS micelles (55), Dodecylphosphocholine micelles (56), and large unilamellar vesicles (53).

Nucleic acid analyses

Comparison between nucleosides and nucleotides

Nucleotides are the main building blocks, which have been used in asymmetric structure of nucleic acids (RNA/DNA). The chiral sugars

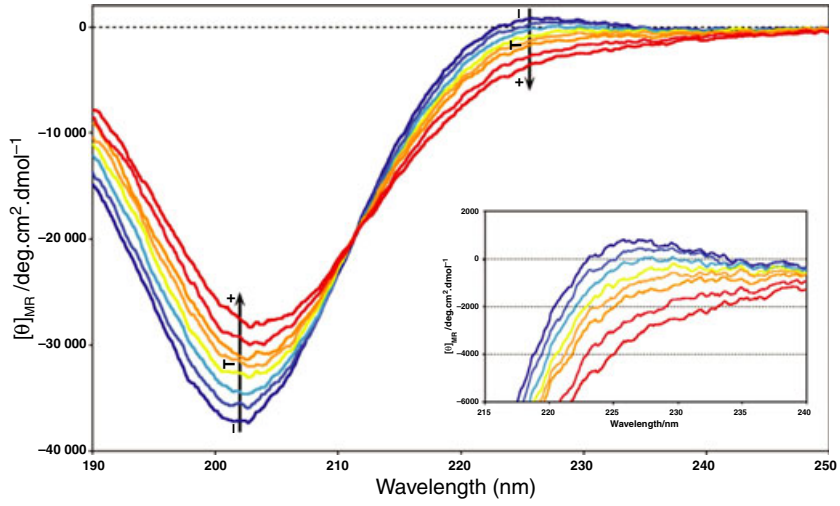

Figure 11: CD spectra of 50 μM SAP at different temperatures (from 0 to 70 °C a spectrum every 10 °C, and at 90 °C) in 10 mM aqueous phosphate buffer at pH 7. Insert: amplification of the region corresponding to the band at 228 nm. The data are adapted from Pujals and Giralt (48).

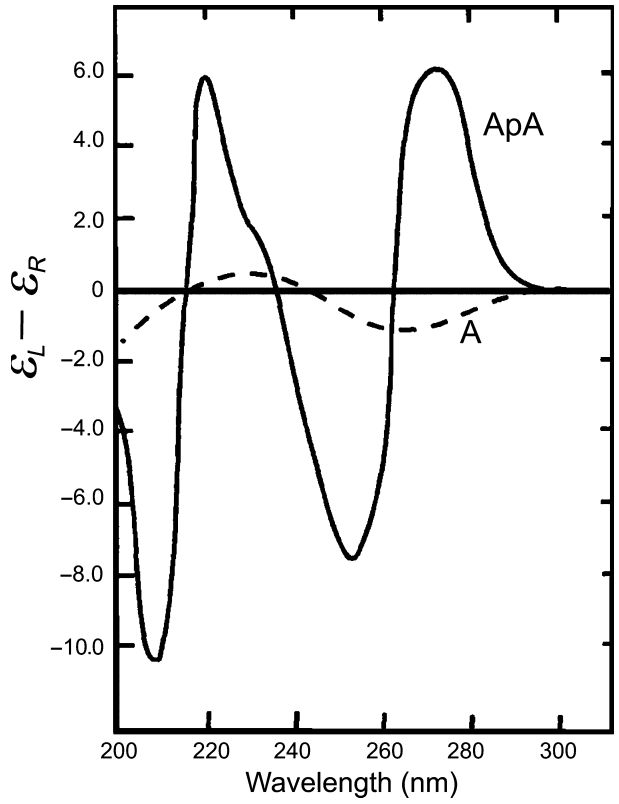

Figure 12: CD spectra of adenylyl-3′-5′-adenosine (ApA) compared with adenosine (A). For both molecules, the spectra are given per mole of nucleoside. The spectra are for aqueous solutions at pH 7 and room temperature. The data are adapted from Warshaw and Cantor (58) and Bloomfield *et al.* (59).

of nucleosides have an intrinsic asymmetry and the interaction of the strong $\pi \rightarrow \pi^*$ transitions of the chromophoric bases with the higher energy in the sugars yield a circular dichroism of low intensity (57). In fact, circular dichroism of nucleic acids is mainly dependent on the stacking geometry of the bases. The difference in CD between a nucleoside, adenosine (A), and a dinucleoside phosphate, adenylyl-3′-5′-adenosine (ApA), is illustrated in Figure 12 (58,59).

CD of the dinucleoside phosphate per adenosine is about a factor of 10 larger than the CD of adenosine. In adenosine, the CD depends on the interaction of adenine with its ribose and phosphate groups; whereas in the dinucleoside phosphate, the CD is mainly originated from the chiral adenine–adenine interaction (58,59). The combination of positive and negative extrema on either side of 260 nm is called an exciton band; there is another exciton band at 215 nm. The positive signs (long wavelength component positive, short wavelength component negative) of these two bands indicate that the two adenines are forming a right-handed stack in ApA (58–60).

Determination of nucleic acid conformations

The circular dichroism spectra of A-RNA, A-DNA, B-DNA and Z-DNA in the 200–320 nm range are shown in Figure 13 (59,61–64).

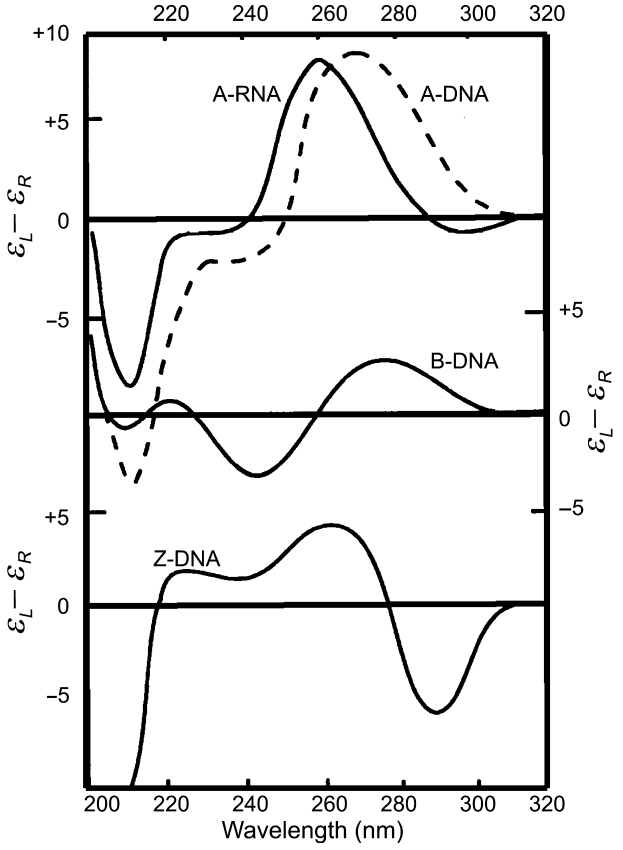

Figure 13: Circular dichroism spectra above 200 nm for right-handed A-RNA and A-DNA, right-handed B-DNA, and left-handed Z-DNA (units are per M/cm/mol of nucleotide) [The data are adapted from Bloomfield *et al.* (59)]. The A-RNA is *Penicillium chrysogenum* fungal virus double-stranded RNA with a G + C content of 54%; it is in 0.01 M Na^+, pH 7 [The data are adapted from Gray *et al.* (61)]. The A-DNA is from *E. coli* with G + C content of 50%; it is in 80% trifluoroethanol, 0.667 M phosphate, pH 7 [The data are adapted from Sprecher *et al.* (62)]. The B-DNA is from *E. coli* DNA in 0.02 M Na^+, pH 7 [The data are adapted from Gray *et al.* (63)]. The Z-DNA is poly [d(CG) d(CG)] in 2 M NaClO, pH 7 [The data are adapted from Riazance *et al.* (64)].

Both A-RNA and A-DNA have spectra that are similar in shape. The A-RNA has a maximum near 260 nm, a minimum near 210 nm, and a small negative CD between 290 and 300 nm. The A-DNA has a maximum at 270 nm, a minimum near 210 nm and zero CD at 300 nm and beyond (59,61). B-DNA has a conservative CD spectrum above 220 nm with approximately equal positive (275 nm) and negative (245 nm) components centred around 260 nm (59,62).

The B-DNA maximum has less than one-half the magnitude of the A-DNA maximum. Of course, the exact shapes and magnitudes of the CD spectra will depend on the base sequences, but the overall patterns will remain constant (59,64). The Z-DNA has a conservative spectrum above 240 nm with approximately equal negative (290 nm) and positive (260 nm) components centred around 280 nm (59,63).

Using vacuum CD has been shown that the right-handed nucleic acids (A-DNA, B-DNA, A-RNA) have an intense positive peak near 186 nm and negative CD below 180 nm; the left handed molecules (Z-DNA, Z-RNA) have an intense negative peak at 190–195 nm, a crossover at 184 nm, and a positive peak below 180 nm (59,64). Calculations of CD spectra for sequences other than those measured show that below 220- nm right-handed double helices have a positive CD couplet and left-handed duplexes have a negative couplet. Therefore, a good method to establish the sense of a duplex helix is to measure the circular dichroism in the wavelength range from 170 to 220 nm (59,64,65).

In summary, CD is most useful technique to compare DNA or RNA conformations and to detect changes when the solvent or temperature is changed. For example, a variety of changes in conditions (temperature, alcohol solvents, and high salt) have been found to cause decrease in a specific wavelength (i.e., 275 nm) (66–74). However, the assignment of the 'C-form' CD spectrum is crucial since it is often found for DNA in condensed or packaged systems. CD studies of bacteriophage (75,76), adenovirus (77), chromatin (78,79), and nucleosomes (80,81) all suggest that DNA adopts the structure represented by this spectrum under biological conditions (59).

Determination of nucleic acid–ligand interactions

DNA is an obvious target for drug intervention since disruption of its structure clearly will have significant biological implications. For instance, studies on the interaction of cationic porphyrins (as a ligand) and their derivatives with DNA have received interest in recent years (82,83). Particularly, porphyrins have been reported from the viewpoint of their use in photodynamic therapy of cancer cells (84), DNA cleavers (85,86) and as drugs to treat some infectious diseases such as AIDS (87).

The negatively charged phosphate groups along the backbone structure of DNA can bind small molecules through electrostatic interactions, but the major sites of drug binding in double-stranded DNA are the major and minor grooves in the double helical structure and intercalation between the bases (1,88). Many of the drugs used contain aromatic rings, and for instance of such binding, we consider the interaction of DNA with acridine orange, even though acridine orange is not actually a drug (1,88). It is not optically active by itself, but binding to DNA induces optical activity into the molecule. This is because, binding causes the electronic energy states of achiral acridine orange to be coupled with the electronic energy states of chiral DNA. Induced optical activity is quite common when achiral small molecules bind to chiral macromolecules. The CD spectra of acridine orange bound to DNA are shown in Figure 14 for various ratios of (bound dye)/DNA (1,88).

Negative value of $\Delta\varepsilon$ is observed at very low values of (bound dye)/(acridine orange), but as this ratio increases, a large positive band develops (1,88). At the highest ratio shown, both strong negative and positive bands are observed. A molecular interpretation of these results has been developed. At very low concentrations of acridine orange, the binding is through intercalation between the bases, with the acridine orange ring structure parallel to the bases (1,88). This produces a negative induced circular dichroism with a minimum $\Delta\varepsilon$ of about -8/M/cm. As the concentration of the ligand increases, the dye binds to the groove which induces a positive CD with a maximum value of about 30/M/cm. These two induced CD signals are enhanced at higher dye concentrations due to interactions between the electronic energy levels of the bound dye molecules (1,88). This example demonstrates the exquisite sensitivity of the CD spectrum to the nature of the binding process and to the secondary structure of the DNA. Studies with many different types of ligands have been carried out (89,90).

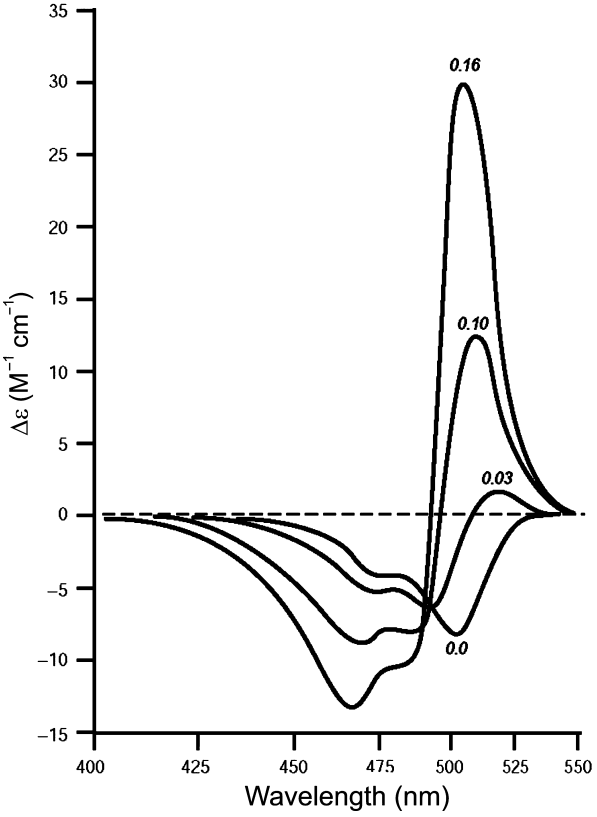

Figure 14: CD per mole of acridine orange bound to DNA at the indicated values of (bound dye)/(DNA). The data are adapted from Fornasiero and Kurucsev (88) and Hammes (1).

Nanostructural analyses

Conformational study of biomolecules upon interacting with nanoparticles

Determining the conformational behaviour of adsorbed biomolecules on a nanoparticles surface using CD deserves some attention (91). Although from a CD spectrum it is not possible to determine exactly whether a biomolecule retains its bioactivity, the degree of protein or nucleic acid denaturing can be estimated by comparing the CD spectra of the native and the surface immobilized one (92). For example, Using CD, Plasma proteins [such as bovine serum albumin (BSA) and human plasma fibrinogen (FNG)] adsorption on various

nanopolymer surfaces was studied and demonstrated that the α-helical contents of BSA and FNG decreased on poly (2-methoxyethylacrylate) (PMEA), PHEMA, and poly(2-ethylhexylacrylate) (PEHA) compared with native BSA and native FNG (92). Consequently, the contents of secondary structures could be analysed quantitatively based on the CD spectra and it was obvious that α-helical contents of native BSA, BSA adsorbed onto the surface of PMEA, PHEMA, and PEHA were 51%, 37%, 15% and 8%, respectively (93).

Similarly, the conformational change of DNA upon interacting with the functionalized nanoparticles has been determined using CD (94,95). As defined, mixed monolayer-functionalized gold nanoparticles present a promising structure for the development of DNA-regulating molecules (96), and have already been shown to be highly effective transfection vectors (96). Some studies revealed that quaternary ammonium-functionalized nanoparticles change the CD signal of DNA to a substantial extent (97). For instance, the amine-terminated cationic nanoparticles (such as NP_L-Phe) denature the DNA secondary structure (Figure 15A), as indicated by the decrease in ellipticity at 280 nm upon addition of nanoparticles (94).

In case of nanoparticles with hydrophobic side chains, CD spectra of the aromatic side chains (i.e. NP_ L-Trp and NP_L-Phe) demonstrate more effective unwinding of the DNA strand in comparison to the aliphatic side chains (i.e. NP_ L-Leu; Figure 15B) (94). This enhanced unwinding arises most likely from π-π stacking of the aromatic rings on the side chains with DNA bases (98). For nanoparticles with hydrophilic side chains, NP_ L-Arg perturbs the DNA structure more than NP_ L-Lys (Figure 15C) (94). This effect can be attributed to the possibility of stable hydrogen bonding between the guanine moiety of arginine and interior DNA bases (94,99).

Information about nanocarriers

CD studies are usual for characterizing of nanocarriers as potential gene/drug delivery devices in nanomedicine and their interactions with biomolecules and drugs have attracted considerable attention in recent studies (100–103). Not only CD often allows one to obtain structural information on the assembled structure of nanocarriers, but also, the CD spectra can predict the efficiency of such nanomaterials in packaging a gene-construct for delivery to a host cell. In addition, conformation analysis of a DNA, before (or after) packaging in a nanocarrier can be monitored by CD (104–108).

When a single chiral group such as aminophenyl propanediol (109) or binaphthyl (110) is located at the core of PBzE dendrimers, the CD data affords information about the variation of the dihedral angle θ in the binaphthyl (111). For fully chiral dendrimers, the chiroptical properties of two series of chiral polyarylether dendrimers from generation 0 to 3 (112) and of dendrimers based on dihydroxypyrrolidine (113) show that the CD spectra change dramatically, indicating conformational substructures in the branches.

The variations in the CD spectra of calf thymus- and linear DNA clearly indicated a transition from B- to A-DNA when exposed to low levels (< 10 μg μL^{-1} solvent) of dendrosomes (Den123; self-organized from amphipathic monomers) (105,113). However, the CD spectral variations in calf thymus- and linear DNA shown a mild

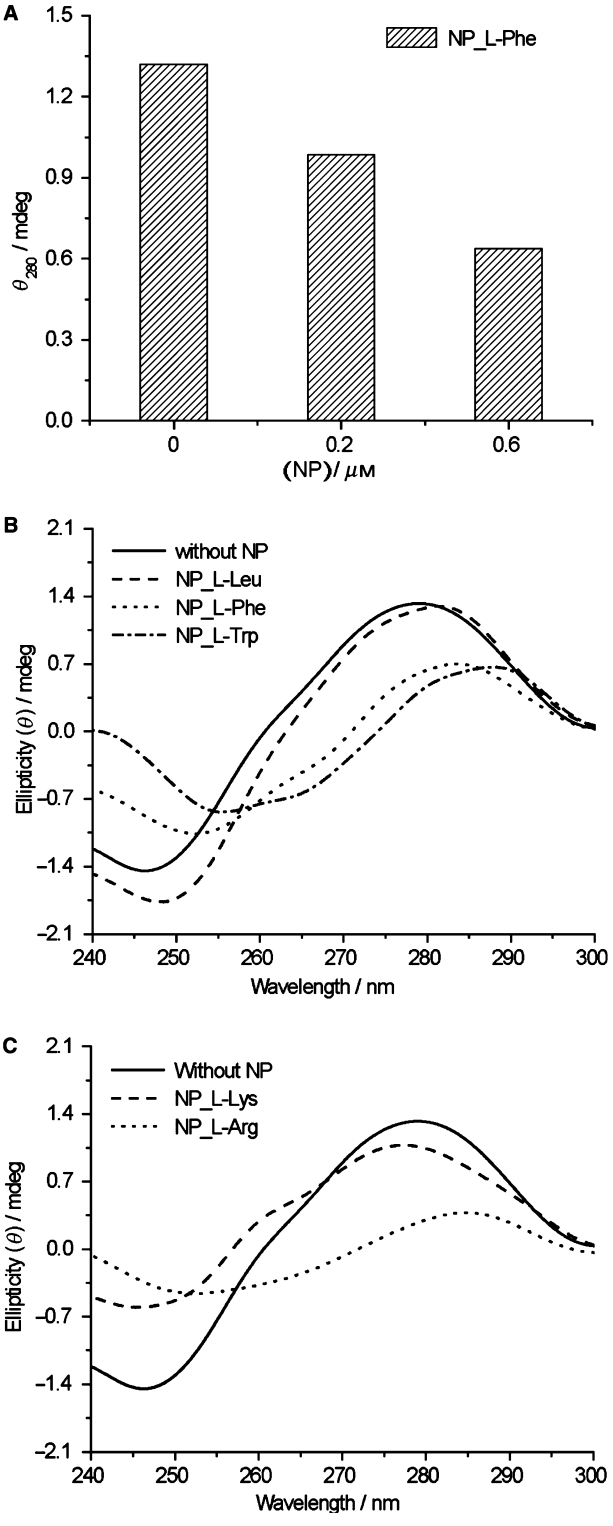

Figure 15: Circular dichroism spectra of 37-mer double-stranded DNA (0.25 μM) in 5 mM AcOH/NaOH buffer (pH 5.0). (A) Decrease in ellipticity at 280 nm (θ_{280}) upon addition of cationic nanoparticles into DNA solution. Change in CD spectra of DNA by (B) hydrophobic nanoparticles and (C) hydrophilic nanoparticles (NP 0.6 μM). The data are adapted from Ghosh *et al.* (94).

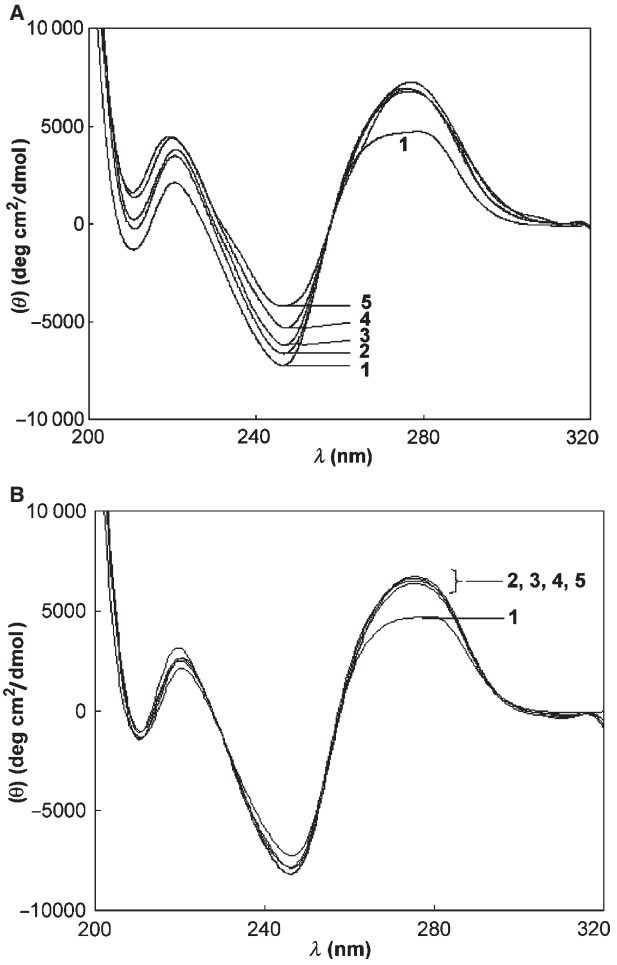

Figure 16: A. CD spectra of calf thymus DNA and its admixtures with Den123 (a self-assembled amphipath) at low level of the latter; (1) DNA alone, (2) Den/DNA:1/17, (3) Den/DNA:1/10, (4) Den/DNA:1/5, (5) Den/DNA:1/1, (6) Den/DNA:5/1. (B) CD spectra of calf thymus DNA and its admixture with Den123 at a high level of the latter; (1) DNA alone, (2) Den/DNA:1/17, (3) Den/DNA:1/10, (4) Den/DNA:1/5, (5) Den/DNA:1/1. The data are adapted from Sadeghizadeh *et al.* (105).

transition from B- to A-DNA (intermediate between A and B-DNA structures) when exposed to higher levels of Den123 (more than 10 μg μL^{-1} solvent) (105) (Figure 16).

CD analyses indicate that DNA is present in the inter-lamellar water space as the DNA is present in the C form as opposed to the more usual B form. A similar change in the conformation of DNA (from B to the C form) was observed upon the entrapment and condensation of DNA into reverse nano-sized micelles formed by non-ionic surfactant (114). If the DNA was present in the central aqueous space, it might be expected that the CD would be largely unchanged from that of the B-form (Figure 17) (115). These changes suggest an alteration in DNA conformation when encapsulated in the vesicles. Similar changes in the CD spectra are observed for DNA encapsulated in vesicles prepared using dipalmitoylphosphatidylcholine and DMPC (114).

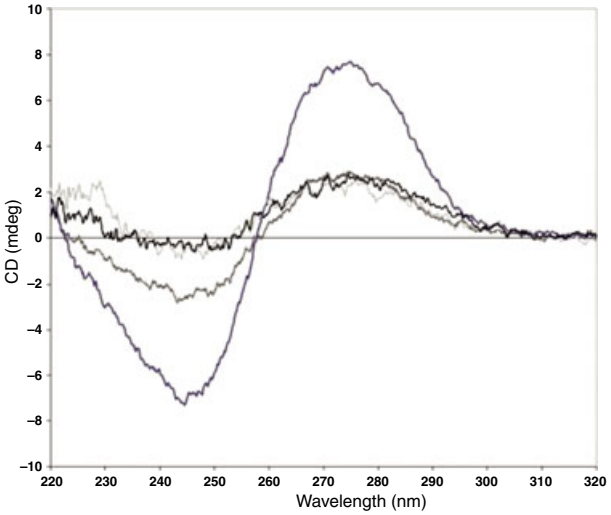

Figure 17: The CD spectrum of free calf thymus DNA in water (present in its usual B-form) is shown in two concentrations, namely 0.01 and 0.025 mg/mL. A significant left shift in the DNA spectrum was observed when the DNA was encapsulated in nanovesicles. The wavelength when the CD recorded changes from being positive to negative shifted from 260 nm for calf thymus DNA in solution to 253 nm for DNA encapsulated in DSPC vesicles. The ratio of the maximum positive to negative CD absorbance for the DNA inside the vesicles was 3.87 compared with 1.1 for calf thymus DNA in solution. The data are adapted from Kudsiova *et al.* (115).

Analysis of DNA biofunctions on nanoparticles

Fabrication of nanowires is showing great potential for future nanodevices (116). In this way, magnetic nanowires are of interest for memory storage devices (117), and metallic nanowires have a high prospective in biosensors (118). Since it is essential to find cost-efficient controlled fabrication processes for these nanostructures (118), a promising way is the utilization of biomolecules at the nano-scale. However, the interaction between biomolecules and nanoparticles has not been known, clearly. Understanding the manipulation of biomolecules will allow controlling the fabrication method of nanowire templating, better. It was demonstrated that DNA has desired properties for templating metal structures (119). Also, it has been shown that DNA can be used for the assembly of magnetic and metallic nanoparticles, creating DNA template nanowires (120). With the use of restriction endonucleases and DNA ligase, it was demonstrated using gel experiments that DNA template nanowires can be clipped at specific sequences and ligated back together (120). In such studies, circular dichroism can be used to examine the mechanism of endonuclease clipping and ligation of the DNA template nanowires (121). For example, enzymatic manipulation of the DNA template for magnetic and metallic nanowires was explored through CD (Figure 18) (122,123).

It was shown at a 1:1 DNA:nanoparticle (NP) ratio, the digested and ligated DNA templates were able to maintain the B-form DNA structure for both metallic and magnetic NP. Also, at NP concentrations >1:5 DNA:NP, CD displayed denaturation and inhibited enzymatic activity (123). Consequently, these phenomena shown that at

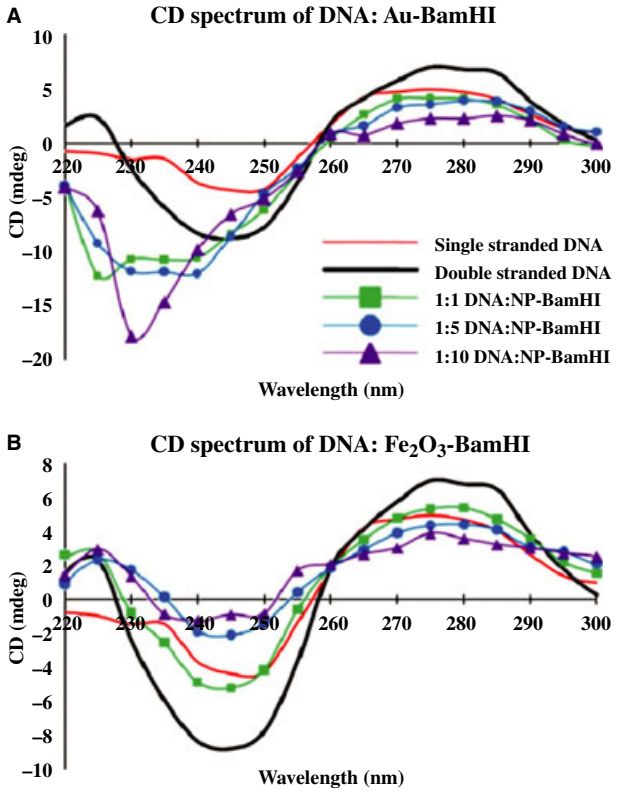

Figure 18: CD spectra of DNA templates at various mass ratios DNA:NP that were clipped with restriction enzyme, *Bam*HI. Colour scheme is for (A) gold NP and (B) Fe_2O_3 NP. CD of templates was measured at room temperature. The data are adapted from Jaganathana and Ivanisevic (123).

high-NP concentration, the DNA template lost its bio-recognition properties, yet, it was able to maintain its double-helix structure and properties at lower concentrations. The results provide significant information on structural alteration and biorecognition effectiveness of the DNA template after enzymatic manipulation (122,123).

CD-Based Techniques

Magnetic circular dichroism

Magnetic circular dichroism spectroscopy is based upon the measurement of the difference in absorption between left circularly polarized (LCP) light and RCP light, induced in a sample by a strong magnetic field oriented parallel to the direction of light propagation (124,125). In fact, the origin of CD and MCD is quite different. Electronic circular dichroism requires a molecular environment where molecular structure features distributed electric charge in a spatial array that has helical handedness. In contrast, MCD is due to electromagnetic interaction of the external field with electronic charge within the sample, no matter how it is distributed, and is a universal property of light absorption for all matter when placed in a magnetic field. Hence, a chiral molecular structure is not a requirement for MCD technique (124,125).

The most important use of MCD spectra in the UV–vis–near-IR region is to assist the interpretation of electronic spectra and provide experimentally based information about the electronic states involved in the observed transitions (124,126). This requires the companion use of absorption spectra, ideally obtained simultaneously and under the same experimental conditions as the MCD spectra. MCD analyses without the companion absorption spectrum can provide nothing more than a fingerprint measurement for the system under experiment (124,126).

In MCD, the sample is placed in a longitudinal magnetic field (i.e. coincident with light propagation axis). It is actually an application of the well-known Faraday effect, the magnetic field induces optical activity in any sort of samples. Magnetic CD is a consequence of the interaction of electronic energy levels with the magnetic field and shows up only when absorption of light occurs (124,125).

As the most extensive applications, electronic and magnetic properties of metalloproteins and inorganic complexes have been studied by MCD (127). There are various studies in the literature have been made on iron-sulphur proteins (128), porphyrins and haeme proteins (129,130), copper, rare earth, cobalt and non-haeme iron bioinorganic systems (131), and non-haeme ferrous enzymes (132) using this technique. Both excited- and ground-state information and a more powerful probe of the coordination geometry and structure of metal chromophores have been provided by employing MCD (127).

Magnetic CD has also been observed for vibrational or rotation–vibrational excitations in the infrared (MVCD) and for magnetic core to valence level absorption edges in the X-ray region (XMCD). It is obvious that the experimental setup for these measurements must be appropriate to the spectral region involved, and therefore, the necessary apparatus will depend upon the wavelength of the light used for the measurement. Infrared or X-ray polarizers and optics are quite different from than those used in the UV-Vis region (124,125).

For XMCD particularly, intense X-ray photon sources are required, which means proximity to synchrotron laboratories is necessary for measurements. Nevertheless, the measured differential absorption between LCP and RCP light by a sample in a strong magnetic field oriented along the propagation direction is entirely analogous to measurements in the UV-Vis, and the origin of MVCD and XMCD likewise results from the Zeeman interaction of the field with magnetic moments within the sample (124,125).

Magnetic vibrational circular dichroism has been developed largely by Keiderling *et al.*, and it was applied initially to vibrational studies of molecules with high symmetries in the condensed phase (124,126). More recently, with improvements in instrumental methods for higher resolution, MVCD was used to study the molecular Zeeman effect (ZE) of rotationally resolved vibrations of small molecules in the gas phase. The infrared measurements necessitated the use of sources and detectors appropriate for the IR region and grid polarizers, lenses, and photo elastic modulator (PEM) elements that have high transmission in the IR (124,133). Since the range of measurement and resolution were greatly enhanced over dispersive

spectrometers, the applications of Fourier transform IR (FTIR) methods to MVCD were also notable. However, the differential signals for LCP and RCP light are often very small and instrumental artefacts have been, and are still, problematic because they can be large compared with the signals of interest (124,133).

Magnetic CD measurements in the X-ray region (XMCD) involve excitation of core electrons to empty or partly filled valence orbitals. For example, the L-edge absorptions in transition metals involve excitation of the spin–orbit split 2p core electrons to the valence 3d or 4p levels. Interpretation of the MCD of these transitions requires experimental measurements that occur typically at energies of hundreds of electron volts (eV) to several thousand electron volts (keV). An interesting feature of XMCD is that it provides an element-specific spectrum that is a measure of orbital and spin angular momentum and the related magnetic properties which result from such momentum. Hence, XMCD has largely involved solid-state samples, often at low temperature (124,125).

Fluorescence detected circular dichroism

Fluorescence detected circular dichroism combines the structural sensitivity and chiral specificity of CD with the sensitivity and specificity of fluorescence (134,135). It consists in measuring the differential emission of light from a sample excited with LCP (left-circularly polarized) and RCP (right-circularly polarized) radiations, and is based on the assumption that the amount of light emitted depends exclusively on the amount absorbed; in other words, the excitation spectrum of the fluorophore parallels the absorption spectrum, and the molecular quantum yield is the same for both circularly polarized components (136). FDCD is then an indirect way of measuring a differential absorption (134,135). It is sensitive to both chiral and fluorescent molecules, and therefore is far more specific than standard transmission CD, because in principle the CD associated with a single fluorophoric molecule or moiety may be selectivity extracted in the presence of many non-fluorescent chromophores. Moreover, similar to the higher sensitivity of fluorescence compared with absorption spectroscopy, the direct measurement of emitted radiation against a zero background renders FDCD more sensitive than conventional CD (137).

In FDCD, the difference in fluorescence intensity for left and RCP excitation is measured. In practice, the technique is very selective, because only fluorophores are detected (even in a multichromophoric molecule). Additionally, exciton coupled FDCD seems a very promising approach, since selectivity and sensitivity are highly enhanced (138,139).

Fluorescence detected circular dichroism helps in separating contributions from multi-component systems, and the quenching detection of chiral molecules also through multidimensional FDCD experiments (140). It could also be employed in numerous examples of mixtures of a fluorophoric probe and a chromophoric species, (i.e., a fluorescent dye associated with a biopolymer), or of a fluorophore inserted into a non-fluorescent chiral biomolecules such as proteins or nucleic acids (140). Fluorescence detected circular dichroism may be applied as a detection tool in chromatography, electrophoresis, and determination of enantiomeric excesses, whereas only a few other reports have provided data regarding FDCD sensitivity enhancement (139,140).

Using a fluorescence cuvette and placing at 90° a second photomultiplier tube with transfer optics, it is possible to collect CD and fluorescence from the sample, simultaneously. Emission signal should be filtered by a long-pass filter, or, alternatively, by an emission monochromator. In fact, the approach is getting today rather popular, mainly in applications requiring long thermal melting experiments to monitor conformational changes, since double information can be obtained, with limited hardware investment (140).

NIR-CD

Applications of circular dichroism in the near-infrared region (NIR) are quite rare, but not uncommon. Many metals linked with proteins and several chiral metal complexes may give CD active bands in the NIR region (NIR is starting from 700 nm up) (141,142). Conventional CD spectroscopies feature double prism monochromators for best efficiency in the far-UV (<250 nm). Double prism monochromators have very low dispersion toward the NIR field, so the actual limit of standard units are around 1100 nm. This wavelength is also the practical NIR limit of red extended (S1) photomultiplier tubes and of Si diodes (141,142). The capability of NIR-CD has been employed by Eglinton *et al.* to show that both the oxidized and reduced states of cytochrome c oxidase (as a metalloprotein) contain electronic states in the NIR region. The spectra have revealed all of the new bands could be assigned with reasonable confidence to one or more of the metal centres in the protein. Consequently, it was clear this spectral region allows observation of the two hems α and $\alpha 3$ separately (143).

To approach the NIR further a different hardware is therefore necessary. Jasco's J-730 was designed for this purpose (144,145), it features a filament source (halogen), a plane grating single monochromator, a linear polarizer, a conventional PEM and a liquid nitrogen cooled in Sb detector. But the most important difference is that a further light modulator (a chopper) must be inserted in the beam, since typical IR detectors would not operate with CD signals (141,142).

Vibrational circular dichroism

Vibrational circular dichroism (VCD) is a spectroscopic technique, which uses circularly polarized light to provide information about a substance (146,147). An interesting feature of many substances is that they respond differently to incident light having different polarization, which they may absorb, reflect, and or transmit different amounts of differently polarized light. VCD technique is generally directed to determining the difference in absorption that a substance exhibits between right and LCP light (148). VCD measurements are particularly useful in the field of stereochemistry, i.e., the study of the shapes of molecules and the spatial arrangement of atoms therein (149). More particularly, VCD analyses are useful in the study of substances which contain chiral molecules (molecules having structures which cannot be superimposed on their mirror images; The concept of chirality is illustrated by a person's right hand, which can be said to be chiral: it is a mirror image of their

left hand, but the hands cannot be superimposed no matter how one orients them relative to each other) (150,151). For example, many substances, particularly biological substances, contains chiral molecules of opposite senses-that is, the molecules are mirror images of each other, in which case they are known as enantiomers or optical isomers. Each of the enantiomers may have different properties, in particular, different biological response (e.g. sugars are chiral molecules, and the human body can digest and use 'right-handed' sugars, but not their left-handed counterparts) (152). Since VCD spectral bands of enantiomers have opposite sign, VCD spectroscopy can allow one to differentiate between enantiomers, a result which is extremely useful in pharmaceutical and chemical fields. Similarly, one can determine how much of one enantiomer is present with respect to its twin, by looking at the spectrum of the mixture of enantiomers and comparing it to one of the pure enantiomers (since the difference will reflect how much the spectrum of one enantiomer attenuates the other) (148,149).

One of VCD-based technique has been improved using IR spectroscopy is FTIR (Fourier transform infrared)-VCD (146). As it was indicated, infrared absorption spectroscopy (IR) is the principal tool available for the study of molecular vibrations (147). Vibrational circular dichroism (VCD) is the differential absorption of left and RCP infrared light by vibrating molecules. The two techniques were combined to create the spectroscopic measurement technique that will be described here, FTIR-VCD (153). FTIR-VCD is used to study the subtle differences in vibrational spectra that result from molecules that differ only in their three dimensional geometry. The technique has been shown to be particularly useful for the study of the conformational characteristics of biological macromolecules such as proteins and nucleic acids and smaller molecules like chiral pharmaceuticals (153).

In summary, the technique can be used in conjunction with calculations (i.e., density functional theory (DFT) calculations) to determine the absolute configuration (AC) of newly synthesized molecules, and can be used to determine enantiomeric purity in molecules whose AC is already known (151). However, if the molecules are enormously large, DFT calculations are impractical. Consequently, biomolecules (e.g. proteins and nucleic acids) cannot be studied. If the molecule is enormously flexible, and the number of populated conformations is enormously large, the prediction of its VCD spectrum becomes very time-consuming and less reliable. Therefore, VCD is not applicable to the determination of ACs. VCD is a practical technique for the majority of medium-sized organic molecules (151).

HPLC- circular dichroism

Presently, pharmaceutical, food and biotechnology companies are facing more and more problems producing enantiomerically pure products. The companies have to verify and certify the purity of their products to meet the regulations that are getting more and more restrictive every day. A large investment is necessary for companies to build commercial-scale production processes for optically pure pharmaceuticals and intermediates. These processes are generally based on various methods such as catalytic asymmetric synthesis, biocatalytic resolution, diastereomeric crystallization, enantioselective absorption or combinations of these methods (154). These processes must include facilities to verify and certify the optical purity of the intermediate and end products or of their metabolites at the laboratory level. For three last decades, HPLC has been the most preferred separation method in these industries (155). Chiral HPLC, both for analytical and preparative scale, is probably the easiest answer to these requests (156). Chiral HPLC separations have been booming through continues development and a growing number of new chiral stationary phases, by the use of chiral modifiers in the mobile phase or by precolumn derivatization with chiral reagents. As well-known enantiomers have the same chemical and physical properties and the only way to discriminate and quantify is their interactions with polarized light, so chiroptical HPLC detectors are the logical complement to any chiral separation (157,158). The tandem combination of chiral and mass-sensitive detectors is very valuable when chromatographic separation can only be partially achieved. This is probably the main appeal of modern chiral HPLC detectors: the possibility to reliably quantify enantiomeric purity without separation is indeed a dramatic advantage. So while these detectors may well be used with chiral columns to verify elution order or to measure (in circular dichroism) the spectra of the compounds, the main interest is to quantify optical purity when using non-chiral chromatographic conditions (159). The capabilities have been applied in several studies (160,161). For instance, Gergely and colleagues have reported the application of HPLC-CD instrument could provide the selective detection of chiral compounds, and subsequently it allowed the employment of high detection wavelengths, presenting more selective detection with minimal background noise (161).

Many important progresses have been achieved in the last few years and various chiral detectors are now commercially available. Jasco has pioneered this field and is today offering chiral detectors based on circular dichroism (e.g. Jasco model OR-2090 Chiral detector; http://www.jasco.co.uk/chiral.asp), which has the unique advantage to provide two different signals (CD and UV) simultaneously, the first proportional to the optical activity and the second related to the mass or amount of the sample compound (162). In addition to dedicated detectors also a conventional CD, equipped with a proper flow cell, can be profitably used for the application, providing chiral and mass information, simultaneously (162).

Stopped-flow circular dichroism

Combination of CD spectroscopies with high mixing speed stopped-flow devices is a well-known technique for fast kinetic measurements (12,163,164). Apart from obvious applications in the organic chemistry field, much interest is now going toward protein folding analyses. For example, Clarcke *et al.* have shown that stopped-flow synchrotron CD can give outstanding information on the kinetics of secondary structure formation. They demonstrated α-helix initiation in peptides is at least 10^5 times slower than expected and long α-helices can fold with an overshoot in helix content (165).

These measurements may be tasking because of multiple shots accumulation may be necessary to extract a valuable result (166). In addition to CD, an instrument equipped with a suitable stopped-flow cell may become the proper optical bench to collect simultaneously absorption and fluorescence data (167).

Proper integration between cell and spectrometer is the first prerequisite, but it is also essential to rely on suitable software to control at the same time both the units. More advanced stopped-flow cells feature today syringes (2, 3 or 4) controlled by stepping-motors, and the possibility to exchange easily the observation cell for different experiments. However, main application of stopped-flow CD is protein folding (166,167).

Synchrotron radiation circular dichroism

Synchrotron radiation circular dichroism is an emerging technique which offers significant improvements to the well-established method of conventional circular dichroism spectroscopy (168). Particularly, developments in instrumentation of CD using vacuum-ultraviolet synchrotron radiation circular dichroism (VUV-SRCD) have made CD a potentially powerful tool in proteomics (169). Using VUV-SRCD, the spectra can be taken at lower range of wavelengths relative to that of conventional CD-spectroscopies. These types of measurements allow us to elucidate finer details of secondary structures of proteins and determine all the predicted folds and motifs in protein secondary structures (170). As a consequence, it takes advantage of the high light flux available from synchrotron sources over a wide range of wavelengths, which results in higher signal-to-noise ratios and enables the collection of lower wavelength data than possible using xenon arc lamps that are typically the illumination source in conventional CDs (171). Therefore considerably smaller amounts of protein are required to obtain a spectrum of comparable quality, and smaller differences can be distinguished (172).

Additionally, averaging times, defined as the times taken at each wavelength to acquire a suitable signal, can be greatly reduced, thereby speeding up the process of obtaining a spectrum. This is advantageous not only for increasing the rate of data collection (useful for structural genomics projects which seek to examine a large number of proteins), but ultimately also for increasing the time resolution of stopped-flow experiments (165).

With SRCD it is possible to collect data <205 nm in almost any solvent and buffer commonly used in biological studies. Thus, this method should provide especially good improvements for assessing secondary structure in protein folding and unfolding studies. Although the technological advancements enabling these measurements were first demonstrated in two last decades (173), growth of applications in structural and functional genomics has been performed more recently (172). For example, applications of SRCD in secondary structure analyses (169), monitoring protein folding and kinetics (165), and drug investigation (169) have been introduced (174).

The applications of SRCD will mainly be divided to investigations of membrane proteins and in the pharmaceutical industry. Integral membrane proteins constitute an important class of proteins that is greatly under-represented in the databases of crystal structures (175). It has been estimated that about one-third of the proteins in the human genome may be membrane-associated, and at present nearly 60% of all drug targets are against membrane proteins. To date, CD studies of membrane proteins have been limited in the accuracy of their secondary structure determinations because none of the reference databases currently available include any membrane proteins, even though it is obvious that such proteins have different spectral characteristics from their soluble ones (176–178). Particularly, with its increased sensitivity and the potential for automation of data collection, SRCD could provide a regular assay for monitoring drug–target interactions (179). Additionally, SRCD is currently being used as a method for examining integrity of protein folding, and may assume an even greater role as more proteins are expressed in high yields as inclusion bodies, requiring refolding to regain their native structures. Indeed, SRCD could find a use as a standard reference method for assays of fidelity of folded products (175).

In summary, SRCD extends the measurements possible with conventional CD instruments, providing much higher information content and the ability to examine biological samples under a richer variety of conditions. On the other hand, the availability of the three-dimensional crystal structure of a protein causally associated with a disease is very valuable in understanding the molecular bases of the disease and in aiding the process of rational drug design for development of pharmaceuticals to treat the disease (180). Knowledge of how the native protein differs from the mutant protein is especially important for this process, although it is not always possible to obtain structures for the mutant proteins, perhaps due to differences in solubility or stability or other characteristics necessary for producing crystals. In this case, SRCD can be used to compare the native and mutant proteins in solution, and in combination with the native protein crystal structure and other biophysics and bioinformatics studies, provide information on the changes associated with the mutant that produces the diseased state (181).

Conclusions

Circular dichroism is a powerful technique for evaluating the conformation of polypeptides and proteins. It is now mature and can be used to tackle more complex problems than those given by the study of small chiral molecules. CD is now routinely used to study biological macromolecules (i.e., proteins, nucleic acids, etc.) and also provides useful structural information. Additionally, recent advances have made it possible to improve the time resolution of natural and magnetically induced CD spectral measurements from the millisecond to nanosecond and picosecond time regimes (182).

One of the goals of systems biology is to discover new emergent properties that may arise from the systemic view used by this discipline in order to understand better the entirety of processes that happen in a biological system (183). Hence, CD techniques would be useful to provide new information about the structural dynamics and electronic states of reaction intermediates (182).

As an analytical instrument, the technology can determine changes in secondary structure in a qualitative and even semi-quantitative fashion. Quantitative analysis of CD spectra for the amount of various secondary structural features is possible, but, as with any assay, the accuracy and proper interpretation of the results depends on an accurate understanding of the procedure.

Since 1970s there have been developed various types of circular dichroism, which their using could improve the structural analyses of a wide range of asymmetric and symmetric substances. On the other hand, from the theoretical view, in the last decades considerable progress has been made in calculating the optical rotation and CD spectra of macromolecules. The extension to larger systems seems highly desirable and should allow the obtainment of precise structural information for macromolecular systems. There are state-of-the-art CD-techniques may have current and future commercial applications in synchrotron end-station design, microfluidics, drug discovery, pharmacology and structural biology.

In conclusion, with the easy availability of a wide range of empirical algorithms for secondary structure calculations, new reference databases and other data analysis tools, CD-based techniques should prove to be even more valuable tools in structural biology over the next decades than CD has been in the past 40 or more years since it was first used to estimate biomolecular structures.

Acknowledgement

The present study was partly supported by Tarbiat modares University and Iranian Nanotechnology Initiative Council (INIC). We are also grateful to Dr. Yaghoub Fathollahi for editing of the manuscript.

References

1. Hammes G.G. (2005) Spectroscopy for the Biological Sciences. New York, USA: John Wiley & Sons, Inc.
2. Berova N., Nakanishi K., Woody R.W. (2000) Circular Dichroism: Principles and Applications, 2nd edn. New York, USA: Wiley-VCH.
3. Fasman G.D. (1996) Circular Dichroism and the Conformational Analysis of Biomolecules. New York, USA: Plenum Publishing Corp.
4. Barrow C.J., Yasuda A., Kenny P.T., Zagorski M.G. (1992) Solution conformations and aggregational properties of synthetic amyloid beta-peptides of Alzheimer's disease. Analysis of circular dichroism spectra. J Mol Biol;225:1075–1093.
5. Hope J., Shearman M.S., Baxter H.C., Chong A., Kelly S.M., Price N.C. (1996) Cytotoxicity of prion protein peptide (PrP106-126) differs in mechanism from the cytotoxic activity of the Alzheimer's disease amyloid peptide, Ah 25–35. Neurodegeneration;5:1–11.
6. Whitmore L., Wallace B.A. (2008) Protein secondary structure analyses from circular dichroism spectroscopy: methods and reference databases. Biopolymers;89:392–400.
7. Velluz L., Legrand M., Grosjean M. (1965) Optical Circular Dichroism: Principles, Measurements and Applications. New York, NY: Academic Press.
8. Abu-Shumays A., Duffield J.J. (1966) Circular dichroism theory and instrumentation. Alnal Chem;38:A29–A58.
9. Hennessey J.P., Johnson W.C. (1981) Information content in the circular dichroism of proteins. Biochemistry;20:1085–1094.
10. Manavalan P., Johnson W.C. Jr (1987) Variable selection method improves the prediction of protein secondary structure from circular dichroism spectra. Anal Biochem;167:76–85.
11. Kelly S.M., Price N.C. (1997) The application of circular dichroism to studies of protein folding and unfolding. Biochim Biophys Acta;1338:161–185.
12. Kelly S.M., Jess T.J., Price N.C. (2005) How to study proteins by circular dichroism. Biochim Biophys Acta;1751:119–139.
13. Kelly S.M., Price N.C. (2000) The use of circular dichroism in the investigation of protein structure and function. Curr Protein Pept Sci;1:349–384.
14. Krell T., Horsburgh M.J., Cooper A., Kelly S.M., Coggins J.R. (1996) Localization of the active site of type II dehydroquinases. Identification of a common arginine-containing motif in the two classes of dehydroquinases. J Biol Chem;271:24492–24497.
15. Purdie N., Swallow K.A., Murphy L.H., Purdies R.B. (1989) Analytical applications of circular dichroism. J Pharma Biomed Anal;7:1519–1526.
16. Kh. Tafreshi N., Hosseinkhani S., Sadeghizadeh M., Sadeghi M., Ranjbar B., Naderi-Manesh H. (2007) The influence of insertion of a critical residue (Arg356) in structure and bioluminescence spectra of firefly luciferase. J Biol Chem;282:8641–8647.
17. Protasevich I., Ranjbar B., Lobachov V., Makarov A., Gilli A., Briand C. (1997) Conformation and thermal denaturation of apocalmodulin: role of electrostatic mutations. Biochemistry;36:2017–2024.
18. Hadizadeh Shirazy N., Ranjbar B., Hosseinkhani S., Khalifeh K., Riahi Madvar A., Naderi-Manesh H. (2007) Critical role of Glu175 on stability and folding of bacterial luciferase: stopped-flow fluorescence study. J Biochem Mol Biol;40:453–458.
19. Hassan Sajedi R., Naderi-Manesh H., Khajeh K., Ranjbar B., Ghaemi N., Naderi-Manesh M. (2004) Purification, characterization, and structural investigation of a new moderately thermophilic and partially calcium-independent extracellular α-amylase from Bacillus sp. TM1. Appl Biochem Biotechnol;119:41–50.
20. Hassan Sajedi R., Taghdir M., Naderi-Manesh H., Khajeh K., Ranjbar B. (2007) Nucleotide sequence, structural investigation and homology modeling studies of a Ca^{2+}-independent α-amylase with acidic pH-profile. J Biochem Mol Biol;40:315–324.
21. Riahi Madvar A., Hosseinkhani S., Khajeh K., Ranjbar B., Asoodeh A. (2005) Implication of a critical residue (Glu175) in structure and function of bacterial luciferase. FEBS Lett;579:4701–4706.
22. Hassani L., Ranjbar B., Khajeh K., Naderi-Manesh H., Naderi-Manesh M., Sadeghi M. (2006) Horseradish peroxidase thermostabilization: the combinatorial effects of the surface modification and the polyols. Enz Microbial Technol;38:118–125.
23. Schulga A., Kurbanov F., Kirpichinikov M., Protasevich I., Lobachov V., Ranjbar B., Chekhov V., Polyakov K., Engelborghs Y., Makarov A. (1998) Comparative study of binase and barnase: experience in chimeric ribonuclease. Protein Eng;11:775–782.
24. Maroufi B., Ranjbar B., Khajeh K., Naderi-Manesh H., Yaghoubi H. (2008) Structural studies of hen egg-white lysozyme dimer: comparison with monomer. Biochim Biophys Acta;1784:1043–1049.

25. Mattice W.L., Riser J.M., Clark D.S. (1976) Conformational properties of the complexes formed by proteins and sodium dodecyl sulfate. Biochemistry;15:4264–4272.
26. Pande V.S., Rokhsar D.S. (1998) Is the molten globule a third phase of proteins? Proc Natl Acad Sci USA;95:1490–1494.
27. Kuwajima K. (2002) The role of the molten globule state in protein folding: the search for a universal view of folding. Proc Ind Natl Sci Acad;68:333–340.
28. Alikhajeh J., Khajeh K., Naderi-Manesh M., Ranjbar B., Sajedi R.H., Naderi-Manesh H. (2007) Kinetic analysis, structural studies and prediction of pKa values of Bacillus KR-8104 α-amylase: The determinants of pH-activity profile. Enz Microb Technol;41:337–345.
29. Mossavarali S., Hosseinkhani S., Ranjbar B., Miroliaei M. (2006) Stepwise modification of lysine residues of glucose oxidase with citraconic anhydride. Int J Biol Macromol;39:192–196.
30. Asghari S.M., Khajeh K., Moradian F., Ranjbar B., Naderi-Manesh H. (2004) Acid-induced conformational changes in Bacillus amyloliquefaciens α-amylase: Appearance of a molten globule like state. Enz Microb Technol;35:51–57.
31. Hosseinkhani S., Ranjbar B., Naderi-Manesh H., Nemat-Gorgania M. (2004) Chemical modification of glucose oxidase: possible formation of molten globule-like intermediate structure. FEBS Lett;561:213–216.
32. Arai M., Kuwajima K. (2000) Role of the molten globule state in protein folding. Adv Protein Chem;53:209–282.
33. Shokri M.M., Khajeh K., Alikhajeh J., Asoodeh A., Ranjbar B., Hosseinkhani S., Sadeghi M. (2006) Comparison of the molten globule states of thermophilic and mesophilic α-amylases. Biophys Chem;122:58–65.
34. Moosavi-Movahedi A.A., Chamani J., Goto Y., Hakimelahi G.H. (2003) Formation of the molten globule-like state of cytochrome c induced by n-alkyl sulfates at low concentrations. J Biochem;133:93–102.
35. Boren K., Andersson P., Larsson M., Carlsson U. (1999) Characterization of a molten globule state of bovine carbonic anhydrase III: loss of asymmetrical environment of the aromatic residues has a profound effect on both the near- and far-UV CD spectrum. Biochim Biophys Acta;1430:111–118.
36. Ptitsyn O.B. (1992) The molten globule state. In: Creighton T.E., editor. Protein Folding. New York: Freeman;pp. 243–300.
37. Langel Ü. (2007) Handbook of Cell-Penetrating Peptides, 2nd edn. USA: Taylor & Francis Group, LLC.
38. Hallbrink M., Floren A., Elmquist A., Pooga M., Bartfai T., Langel U. (2001) Cargo delivery kinetics of cell-penetrating peptides. Biochim Biophys Acta;1515:101–109.
39. Pooga M., Hallbrink M., Zorko M., Langel U. (1998) Cell penetration by transportan. FASEB J;12:67–77.
40. Morris M.C., Depollier J., Mery J., Heitz F., Divita G. (2001) A peptide carrier for the delivery of biologically active proteins into mammalian cells. Nat Biotechnol;19:1173–1176.
41. Morris M.C., Chaloin L., Mery J., Heitz F., Divita G. (1999) A novel potent strategy for gene delivery using a single peptide vector as a carrier. Nucleic Acids Res;27:3510–3517.
42. Morris M.C., Vidal P., Chaloin L., Heitz F., Divita G. (1997) A new peptide vector for efficient delivery of oligonucleotides into mammalian cells. Nucleic Acids Res;25:2730–2736.
43. Koppelhus U., Awasthi S.K., Zachar V., Holst H.U., Ebbesen P., Nielsen P.E. (2002) Cell dependent differential cellular uptake of PNA, peptides, and PNA-peptide conjugates. Antisense Nucleic Acid Drug Dev;12:51–63.
44. Eriksson M., Nielsen P.E., Good L. (2002) Cell permeabilization and uptake of antisense peptide-peptide nucleic acid (PNA) into Escherichia coli. J Biol Chem;277:7144–7147.
45. Koch A.M., Reynolds F., Kircher M.F., Merkle H.P., Weissleder R., Josephson L. (2003) Uptake and metabolism of a dual fluorochrome Tat-nanoparticle in HeLa cells. Bioconjug Chem;14:1115–1121.
46. Tseng Y.L., Liu J.J., Hong R.L. (2002) Translocation of liposomes into cancer cells by cell penetrating peptides penetratin and tat: a kinetic and efficacy study. Mol Pharmacol;62:864–872.
47. Herbig M.E., Weller K.M., Merkle H.P. (2007) Reviewing biophysical and cell biological methodologies in cell-penetrating peptide (CPP) research. Crit Rev Ther Drug Car Sys;24:203–255.
48. Pujals S., Giralt E. (2008) Proline-rich, amphipathic cell-penetrating peptides. Adv Drug Deliv Rev;60:473–484.
49. Rabanal F., Ludevid M.D., Pons M., Giralt E. (1993) CD of proline-rich polypeptides: application to the study of the repetitive domain of maize glutelin-2. Biopolymers;33:1019–1028.
50. Berlose J.P., Convert O., Derossi D., Brunissen A., Chassaing G. (1996) Conformational and associative behaviours of the third helix of antennapedia homeodomain in membrane-mimetic environments. Eur J Biochem;242:372–386.
51. Magzoub M., Eriksson L.E., Graslund A. (2002) Conformational states of the cell-penetrating peptide penetratin when interacting with phospholipid vesicles: effects of surface charge and peptide concentration. Biochim Biophys Acta;1563:53–63.
52. Thoren P.E., Persson D., Esbjorner E.K., Goksor M., Lincoln P., Norden B. (2004) Membrane binding and translocation of cell-penetrating peptides. Biochemistry;43:3471–3489.
53. Magzoub M., Eriksson L.E., Graslund A. (2003) Comparison of the interaction, positioning, structure induction and membrane perturbation of cell-penetrating peptides and non-translocating variants with phospholipid vesicles. Biophys Chem;103:271–288.
54. Persson D., Thoren P.E., Lincoln P., Norden B. (2004) Vesicle membrane interactions of penetratin analogues. Biochemistry;43:11045–11055.
55. Lindberg M., Jarvet J., Langel U., Graslund A. (2001) Secondary structure and position of the cell-penetrating peptide transportan in SDS micelles as determined by NMR. Biochemistry;40:3141–3149.
56. Barany-Wallje E., Andersson A., Graslund A., Maler L. (2004) NMR solution structure and position of transportan in neutral phospholipid bicelles. FEBS Lett;567:265–269.
57. Van Holde K.E., Johnson W.C., Ho P.S. (1998) Principle of Physical Biochemistry. New Jersey, USA: Prentice-Hall Inc., p. 418–451.
58. Warshaw M.M., Cantor C.R. (1970) Oligonucleotide interactions. IV. Conformational differences between deoxy- and ribodinucleoside phosphates. Biopolymers;9:1079–1103.
59. Bloomfield V.A., Crothers D.M., Tinoco I. Jr, with contribution from, Hearst J.E., Wemmer D.E., Kollman P.A., Turner D.H. (2000) Nucleic Acids: Structures, Properties, and Functions. Sausalito, California, USA: University Science Books.

60. Bush C.A., Tinoco I. Jr (1967) Calculation of the optical rotatory dispersion of dinucleoside phosphates. Appendix. Derivation of the ORD and CD curves from absorption and rotational strengths. J Mol Biol;23:601–614.
61. Gray D.M., Liu J.-J., Ratliff R.L., Allen F.S. (1981) Sequence dependence of the circular dichroism of synthetic double-stranded RNAs. Biopolymers;20:1337–1382.
62. Sprecher C.A., Baase W.A., Johnson W.C. Jr (1979) Conformation and circular dichroism of DNA. Biopolymers;18:1009–1019.
63. Gray D.M., Taylor T.N., Lang D. (1978) Dehydrated circular DNA: Circular dichroism of. molecules in ethanolic solutions. Biopolymers;17:145–157.
64. Riazance J.H., Baase W.A., Johnson W.C. Jr, Hall K., CNZ P., Tinoco I. Jr (1985) Evidence for Z-Form RNA by vacuum UV-circular dichroism. Nucleic Acids Res;13:4983–4989.
65. Gray D.M., Johnson K.H., Vaughan M.E., Morris P.A., Sutherland J.C., Ratliff R.L. (1990) The vacuum VCD bands of repeating DNA sequences are dependent on sequence and conformation. Biopolymers;29:317–323.
66. Williams A.L. Jr, Cheong C., Tinoco I. Jr, Clark L.B. (1986) Vacuum ultraviolet circular dichroism as an indicator of helical handedness in nucleic acids. Nucleic Acids Res;14:6649–6659.
67. Nelson R.G., Johnson W.C.. Jr (1970) Conformation of DNA in ethylene glycol. Biochem Biophys Res Commun;41:211–216.
68. Gennis R.B., Cantor C.R. (1972) Optical studies of a conformational change in DNA before melting. J Mol Biol;65:381–399.
69. Studdert D.S., Patroni M., Davis R.C. (1972) Circular dichroism of DNA: temperature and salt dependence. Biopolymers (Pept. Sci.);11:761–779.
70. Ivanov V.I., Minchenkova L.E., Schyolkina A.K., Poletayev A.I. (1973) Different conformations of double-stranded nucleic acid in solution as revealed by circular dichroism. Biopolymers (Pept. Sci.);12:89–110.
71. Ivanov V.I., Minchenkova L.E., Minyat E.E., Frank-Kamonetshii M.D., Schyolkina A.K. (1974) The B to A transition of DNA in solution. J Mol Biol;87:817–833.
72. Girod J.C., Johnson W.C. Jr, Huntington S.K., Maestre M.F. (1973) Conformation of deoxyribonucleic acid in alcohol solutions. Biochemistry;12:5092–5096.
73. Johnson W.C. Jr, Girod J.C. (1974) A novel denaturation of DNA. Biochim Biophys Acta;353:193–199.
74. Hanlon S., Brudno S., Wu T.T., Wolf B. (1975) Structural transitions of deoxyribonucleic acid in aqueous electrolyte solutions. I. Reference spectra of conformational limits. Biochemistry;14:1648–1660.
75. Maestre M.F., Gray D.M., Cook R.B. (1971) Magnetic circular dichroism study on synthetic polynucleotides, bacteriophage structure, and DNA's. Biopolymers (Pept. Sci.);10:2537–2553.
76. Dorman B.P., Maestre M.F. (1973) Experimental differential light-scattering correction to the circular dichroism of bacteriophage T2. Proc Natl Acad Sci USA;70:255–259.
77. Baase W.A., Johnson W.C.. Jr (1979) Circular dichroism and DNA secondary structure. Nucleic Acids Res;6:797–814.
78. Shih T.Y., Fasman D.G. (1970) Conformation of deoxyribonucleic acid in chromatin: A circular dichroism study. J Mol Biol;52:125–129.
79. Hanlon S., Johnson R.S., Wolf G., Chan A. (1972) Mixed conformations of deoxyribonucleic acid in chromatin: a preliminary report. Proc Natl Acad Sci USA;69:3263–3267.
80. Lawrence J.-J., Chan D.C.F., Piette L.H. (1976) Conformational state of DNA in chromatin subunits. Circular dichroism, melting, and ethidium bromide binding analysis. Nucleic Acids Res;3:2879–2893.
81. Rill R., Van Holde K.E. (1973) Properties of nuclease-resistant fragments of calf thymus chromatin. J Biol Chem;248:1080–1083.
82. Asadi M., Safaei E., Ranjbar B., Hasani L. (2005) A study on the binding of two water-soluble tetrapyridinoporphyrazinato copper(II) complexes to DNA. J Mol Struct;754:116–123.
83. Asadi M., Safaei E., Ranjbar B., Hasani L. (2004) Thermodynamic and spectroscopic study on the binding of cationic ZD(II) and Co(II) tetrapyridinoporphyrazines to calf thymus DNA: The role of the central metal in binding parameters. New J Chem;28:1227–1234.
84. Fiel R.J., Datta-Gupta N., Mark E.H., Howard J.C. (1981) Induction of DNA damage by porphyrin photosensitizers. Cancer Res;41:3543–3545.
85. Prasueth D., Gaudemer A., Verlhac J., Kraljic I., Sissoeff I., Guille E. (1986) Photocleavage of DNA in presence of synthetic water-soluble porphyrins. Photochem Photobiol;44:717–724.
86. Magda D., Wright M., Miller R.A., Sessler J.L., Sansom P.I. (1995) Sequence-Specific Photocleavage of DNA by an Expanded Porphyrin with Irradiation above 700 nm. J Am Chem Soc;117:3629–3630.
87. Dixon D.W., Schinazi R., Marzilli L.G. (1990) Porphyrins as agents against the human immunodeficiency virus. Ann NY Acad Sci;616:511–513.
88. Fornasiero D., Kurucsev T. (1981) Circular dichroism spectra and the interaction between acridine dyes and deoxyribonucleic acid. J Phys Chem;85:613–618.
89. Safaei E., Ranjbar B., Hasani L. (2007) A study of the assembly of Fe(II) and dual binding of Ni(II) porphyrazines on CT-DNA. J Porphyrins Phthalocyanines;11:805–814.
90. Bathaie S.Z., Bolhasani A., Hoshyar R., Ranjbar B., Sabouni F., Moosavi-Movahedi A.-A. (2007) Interaction of saffron carotenoids as anticancer compounds with ctDNA, oligo $(dG.dC)_{15}$, and oligo $(dA.dT)_{15}$. DNA Cell Biol;26:533–540.
91. Liu H., Webster T.J. (2007) Nanomedicine for implants: A review of studies and necessary experimental tools. Biomaterials;28:354–369.
92. Tziampazis E., Kohn J., Moghe P.V. (2000) PEG-variant biomaterials as selectively adhesive protein templates model surfaces for controlled cell adhesion and migration. Biomaterials;21:511–520.
93. Tanaka M., Motomura T., Kawada M., Anzai T., Kasori Y., Shiroya T., Shimura K., Onishi M., Mochizuki A. (2000) Blood compatible aspects of poly (2-methoxyethylacrylate) (PMEA) relationship between protein adsorption and platelet adhesion on PMEA surface. Biomaterials;21:1471–1481.
94. Ghosh P.S., Han G., Erdogan B., Rosado O., Krovi S.A., Rotello V.M. (2007) Nanoparticles featuring amino acid-functionalized side chains as DNA receptors. Chem Biol Drug Design;70:13–18.

95. Goodman C.M., Chari N.S., Han G., Hong R., Ghosh P., Rotello V.M. (2006) DNA-binding by functionalized gold nanoparticles: mechanism and structural requirements. Chem Biol Drug Design;67:297–304.
96. Goodman C.M., Rotello V.M. (2004) Biomacromolecule surface recognition using nanoparticles. Mini Rev Org Chem;1:103–114.
97. Sandhu K.K., McIntosh C.M., Simard J.M., Smith S.W., Rotello V.M. (2002) Gold nanoparticle-mediated transfection of mammalian cells. Bioconjug Chem;13:3–6.
98. Kikuta E., Murata M., Katsube N., Koike T., Kimura E. (1999) Novel recognition of thymine base in double-stranded DNA by zinc(II)-macrocyclic tetraamine complexes appended with aromatic groups. J Am Chem Soc;121:5426–5436.
99. Hermann T., Patel D.J. (2000) Biochemistry - adaptive recognition by nucleic acid aptamers. Science;287:820–825.
100. Zhang X.G., Teng D.Y., Wu Z.M., Wang X., Wang Z., Yu D.M., Li C.X. (2008) PEG-grafted chitosan nanoparticles as an injectable carrier for sustained protein release. J Mater Sci: Mater Med;19:3525–3533.
101. Wang X.H., Goh S.H.Z.H., Lee S.Y., Wu C. (1999) Light-scattering characterization of fullerene-containing poly(alkyl methacrylate)s in THF. Macromolecules;32:2786–2788.
102. Singh J., Dutta P.K. (2008) Spectroscopic and conformational study of chitosan acid salts. J Polym Res;8:9221–9223.
103. Kissmann J., Ausar S.F., Foubert T.R., Brock J., Switzer M.H., Detzi E.J., Vedvick T.S., Middaugh C.R. (2008) Physical stabilization of norwalk virus-like particles. J Pharm Sci;97:4208–4218.
104. Caminade A.-M., Laurent R., Majoral J.-P. (2005) Characterization of dendrimers. Adv Drug Deliv Rev;57:2130–2146.
105. Sadeghizadeh M., Ranjbar B., Damaghi M., Khaki L., Sarbolouki M.N., Najafi F., Parsaee S., Ziaee A.-A., Massumi M., Lubitz W., Kudela P., Paukner S., Karami A. (2008) Dendrosomes as novel gene porters-III. J Chem Technol Biotechnol;83:912–920.
106. Xu Y., Szoka F.C.. Jr (1996) Mechanism of DNA release from cationic liposome–DNA complexes used in cell transfection. Biochemistry;35:5616–5623.
107. Chaumette J.L., Laufersweiler M.J., Parquette J.R. (1998) Synthesis and chiroptical properties of dendrimers elaborated from a chiral, nonracemic central core. J Org Chem;63:9399–9405.
108. Yevdokimov Y.M., Salyanov V.I. (2003) Liquid crystalline dispersions of complexes formed by chitosan with double-stranded nucleic acids. Liq Cryst;30:1057–1074.
109. Chen Y.M., Chen C.F., Xi F. (1998) Chiral dendrimers with axial chirality. Chirality;10:661–666.
110. Rosini C., Superchi S., Peerlings H.W.I., Meijer E.W. (2000) Enantiopure dendrimers derived from the 1,1V-binaphthyl moiety: a correlation between chiroptical properties and conformation of the 1,1V-binaphthyl template. Eur J Org Chem;2000:61–71.
111. Murer P., Seebach D. (1995) Synthesis and properties of first to third generation dendrimers with doubly and triply branched chiral building blocks. Angew Chem Int Ed Engl;34:2116–2119.
112. Cicchi S., Goti A., Rosini C., Brandi A. (1998) Enantiomerically pure dendrimers based on a trans-3,4-dihydroxypyrrolidine. Eur J Org Chem;11:2591–2597.
113. Dennig J., Duncan E. (2002) Gene transfer into eukaryotic cells using activated polyamidiamine dendrimers. J Biotechnol;90: 339–347.
114. Budker V.G., Slattum P.M., Monahan S.D., Wolff J.A. (2002) Entrapment and condensation of DNA in neutral reverse micelles. Biophys J;82:1570–1579.
115. Kudsiova L., Arafiena C., Lawrence M.J. (2008) Characterization of chitosan-coated vesicles encapsulating DNA suitable for gene delivery. J. Pharma Sci;97:3981–3997.
116. Gu Q., Cheng C., Gonela R., Suryanarayanan S., Anabathula S., Dai K., Haynie D.T. (2006) DNA nanowire fabrication. Nanotechnol;17:R14–R25.
117. Yogeswaran U., Chen S. (2008) A review on the electrochemical sensors and biosensors composed of nanowires as sensing material. Sensors;8:290–313.
118. Li Y., Qian F., Xiang J., Lieber C.M. (2006) Nanowire electronic and optoelectronic devices. Mater Today;9:18–27.
119. Braun E., Eichen Y., Sivan U., Ben-Yoseph G. (1998) DNA-templated assembly and electrode attachment of a conducting silver wire. Nature;391:775–778.
120. Kinsella J.M., Ivanisevic A. (2007) DNA-templated magnetic nanowires with different compositions: fabrication and analysis. Langmuir;23:3886–3890.
121. Kinsella J.M., Ivanisevic A. (2005) Enzymatic clipping of DNA wires coated with magnetic nanoparticles. J Am Chem Soc;127:3276–3277.
122. Kinsella J.M., Shalaev M.W., Ivanisevic A. (2007) Ligation of nanoparticle coated DNA cleaved with restriction enzymes. Chem Mater;19:3586–3588.
123. Jaganathana H., Ivanisevic A. (2008) Circular dichroism study of enzymatic manipulation on magnetic and metallic DNA template nanowires. Colloids Surf B Biointerf;67:279–283.
124. Mason W.R. (2007) A Practical Guide to Magnetic Circular Dichroism Spectroscopy. New York, USA: John Wiley & Sons, Inc.
125. Ball D.W. (1991) An introduction to magnetic circular dichroism spectroscopy; general theory and applications. Spectroscopy;6:18–24.
126. Funk T., Deb A., George S.J., Wang H., Cramer S.P. (2005) X-ray magnetic circular dichroism-a high energy probe of magnetic properties. Coord Chem Rev;249:3–30.
127. Johnson M.K. (2000) CD and MCD spectroscopy. In: Que L. Jr, editor. Physical Methods in Bioinorganic Chemistry: Spectroscopy and Magnetism. Sausalito, California: University Science Books;p. 233–285.
128. Johnson M.K., Robinson A.E., Thomson A.J. (1982) Low-temperature magnetic circular dichroism of iron-sulfur proteins. In: Spiro T.G., editor. Iron-Sulfur Proteins. New York: Wiley;p. 367–406.
129. Dawson J.H., Dooley D.M. (1989) Magnetic circular dichroism spectroscopy of iron porphyrins and heme proteins. In: Lever A.B.P., Gray H.B., editors. Iron Porphyrins, Part 3. New York: VCH Publishers;p. 1–92.
130. Cheesman M.R., Greenwood C., Thomson A.J. (1991) Magnetic circular dichroism of hemoproteins. In: Sykes AG, ed. Advances in Inorganic Chemistry. Vol. 36, San Diego, CA: Academic; p. 230–255.
131. Dooley D.M., Dawson J.H. (1984) Bioinorganic applications of magnetic circular dichroism spectroscopy: copper, rare-earth ions, cobalt and non-heme iron systems. Coord Chem Rev;60:1–66.

132. Solomon E.I., Pavel E.G., Loeb K.E., Campochiaro C. (1995) Magnetic circular dichroism spectroscopy as a probe of the geometric and electronic structure of non-heme ferrous enzymes. Coord Chem Rev;144:369–460.
133. Cramer S.P. (2003) ACS symposium series 858 paramagnetic resonance of metallobiomolecules. 358–364.
134. Tam C.N., Bour P., Keiderling T.A. (1996) Observations of rotational magnetic moments in the ground and some excited vibrational $\sum$ states of C_2H_2, C_2HD, and C_2D_2 by magnetic vibrational circular dichroism. J Chem Phys;104:1813–1824.
135. Tinoco I.. Jr, Turner D.H. (1976) Fluorescence detected circular dichroism. Theory. J Am Chem Soc;98:6453–6456.
136. Turner D.H. (1978) Fluorescence-detected circular dichroism. Methods Enzymol;49:199–214.
137. Tran C.D., Fendler J.H. (1979) Stereoselective energy transfer induced by circularly polarized light. J Am Chem Soc;101:1285–1288.
138. Harada N., Nakanishi K. (1983) Circular Dichroic Spectroscopy-Exciton Coupling in Organic Stereochemistry. Mill Valley, CA: University Science Books.
139. Dong J.G., Wada A., Takahashi T., Nakanishi K., Berova N. (1997) Sensitivity enhancement of exciton coupling by fluorescence detected circular dichroism (FDCD). J Am Chem Soc;119:12024–12025.
140. Tanaka K., Pescitelli G., Nakanishi K., Berova N. (2005) Fluorescence detected exciton coupled circular dichroism: development of new fluorescent reporter groups for structural studies. Monatshefte fur Chemie;136:367–395.
141. Ramsay G., Eftink M.R. (1994) A multidimensional spectrophotometer for monitoring thermal unfolding transitions of macromolecules. Biophys J;31:516–523.
142. Keiderling T.A. (1990) Vibrational CD: Comparison of Techniques and Practical Considerations, in Practical Fourier Transform Infrared Spectroscopy. New York, USA: Academic Press;p. 203–284.
143. Eglinton D.G., Johnson M.K., Thomson A.J., Gooding P.E., Greenwood C. (1980) Near-infrared magnetic and natural circular dichroism of cytochrome *c* oxidase. Biochem J;191:319–331.
144. Oberg K.A., Ruysschaert J.M., Goormaghtigh E. (2004) The optimization of protein secondary structure determination with infrared and circular dichroism spectra. Eur J Biochem;271: 2937–2948.
145. Fujii H., Finnegan M.G., Miki T., Crouse B.R., Kakinuma K., Johnson M.K. (1995) Spectroscopic identification of the heme axial ligation of cytochrome b558 in the NADPH oxidase of porcine neutrophils. FEBS Lett;377:345–348.
146. Kudo K., Nonokawa D., Li J., Shiraishi S. (2002) Synthesis of optically active alicyclic polyimides from a chiral, nonracemic dianhydride. J PolymSci Part A: PolymChem;40:4038–4044.
147. Nafie L.A., Cheng J.C., Stephens P.J. (1975) Vibrational circular dichroism of 2,2,2-trifluoro-1-phenylethanol. J Am Chem Soc;97:3842–3843.
148. Nafie L.A., Keiderling T.A., Stephens P.J. (1976) Vibrational circular dichroism. J Am Chem Soc;98:2715–2723.
149. Keiderling T.A., Stephens P.J. (1976) Vibrational circular dichroism of overtone and combination bands. Chem Phys Lett;41:46–48.
150. Keiderling T.A., Stephens P.J. (1977) Vibrational circular dichroism of dimethyl tartrate. A coupled oscillator. J Am Chem Soc;99:8061–8062.
151. Stephens P.J., Devlin F.J., Pan J.-J. (2008) The determination of the absolute configurations of chiral molecules using vibrational circular dichroism (VCD) spectroscopy. Chirality;20:643–663.
152. Chen G.-C., Polavarapu P.L., Weibel S. (1994) New design for Fourier transform infrared vibrational circular dichroism spectrometers. Appl Spectrosc;48:1218–1223.
153. Yoo R.K., Croatto P.V., Wang B., Keiderling T.A. (1991) A method for the determination of the zero-path-difference position in a fourier transform infrared spectrometer: application to magnetic vibrational circular dichroism. Appl Spectrosc;45:231–236.
154. Reetz M.T., Kuhling K.M., Hinrichs H., Deege A. (2000) Circular dichroism as a detection method in the screening of enantioselective catalysts. Chirality;12:479–482.
155. Drake A.F., Gould J.M., Mason S.F. (1980) Simultaneous monitoring of ligh-absorption and optical activity in the liquid chromatography of chiral substance. J Chromatogr;202:239–245.
156. Salvadori P., Rosini C., Bertucci C. (1984) Circular dichroic detection in the HPLC of chiral molecules: direct determination of elution orders. J Org Chem;49:5050–5054.
157. Salvadori P., Bertucci C., Rosini C. (1991) Circular dichroism detection in HPLC. Chirality;3:376–385.
158. Goodall D.M. (1993) Chiral analysis based on polarimetric detection. Trends Anal Chem;12:177–184.
159. Brandl F., Pustet N., Mannschreck A. (1999) Applications of a novel type of detector for liquid chromatography of chiral compounds. Int Lab;29:10C–15C.
160. Gergely A., Zsila F., Horva'th P., Szász G. (1999) Determination of absolute configuration of ketamine enantiomers by HPLC-CD-UV technique. Chirality;11:741–744.
161. Gergely A., Szász G., Szentesi A., Gyimesi-Forrás K., Kökösi J., Szegvári D., Veress G. (2006) Evaluation of CD detection in an HPLC system for analysis of DHEA and related steroids. Anal Bioanal Chem;384:1506–1510.
162. Bertucci C., Andrisano V., Cavrini V., Castiglioni E. (2000) Reliable assay of extreme enantiomeric purity values by a new circular dichroism based HPLC detection system. Chirality;12:84–92.
163. Khalifeh K., Ranjbar B., Khajeh K., Naderi-Manesh H., Sadeghi M., Gharavi S. (2007) A stopped-flow fluorescence study of the native and modified lysozyme. Biologia;62:258–264.
164. Noppert A., Gast K., Zirwer D., Damaschun G. (1998) Initial hydrophobic collapse is not necessary for folding RNase A. Folding & Design;3:213–221.
165. Clarke D.T., Doig A.J., Stapeley B.J., Jones G.R. (1999) The alpha-helix folds on a millisecond time scale. Proc Natl Acad Sci USA;96:7232–7237.
166. Bayley P.M. (1981) Stopped-flow circular dichroism techniques: scope and limitations. Prog Biophys Mol Biol;37:149–180.
167. Kuwajima K., Fasman G.D. (1996) Stopped-Flow CD in Circular Dichroism and the Conformational Analysis of Biomolecules. New York, USA: Plenum Press.
168. Wallace B.A. (2000) Synchrotron radiation circular-dichroism spectroscopy as a tool for investigating protein structures. J Synchrotron Radiat;7:289–295.
169. Wallace B.A., Janes W.R. (2001) Synchrotron radiation circular dichroism spectroscopy of proteins: secondary structure, fold

recognition and structural genomics. Curr Opin Chem Biol;5:567–571.
170. Khalifeh K., Ranjbar B. (2005) A novel application of quantum dots as a tool for storage of CD spectra data in proteomics. Med Hypotheses;65:821–822.
171. Lees J.G., Wallace B.A. (2002) Synchrotron radiation circular dichroism and conventional circular dichroism spectroscopy: A comparison. Spectroscopy;16:121–125.
172. Wallace B.A. (2000) Conformational changes by synchrotron radiation circular dichroism spectroscopy. Nat Struct Biol;7: 708–709.
173. Sutherland J.C., Desmond E.J., Takacs P.Z. (1980) Versatile spectrometer for experiments using synchrotron radiation at wavelengths greater than 100 nm. Nucl Instr Methods;172:195–199.
174. Wallace B.A., Wien F., Miles A.J., Lees J.G., Hoffmann S.V., Evans P., Wistowc G.J., Slingsby C. (2004) Biomedical applications of synchrotron radiation circular dichroism spectroscopy: Identification of mutant proteins associated with disease and development of a reference database for fold motifs. Faraday Discuss;126:237–243.
175. Cascio M., Wallace B.A. (1994) Red- and blue-shifting in the circular dichroism spectra of polypeptides due to dipole effects. Protein Pept Lett;1:136–140.
176. Cascio M., Wallace B.A. (1995) Effects of local environment on the circular dichroism spectra of polypeptides. Anal Biochem;227:90–100.
177. Blundell T.L., Mizuguchi K. (2000) Structural genomics: an overview. Prog Biophys Mol Biology;73:289–295.
178. Rodi D.J., Janes R.W., Sangasnee H.J., Soares A., Holton R.A., Wallace B.A., Makowski L. (1999) Screening of a library of phage-displayed peptides identifies human Bcl-2 as a Taxol-binding protein. J Mol Biol;285:197–203.
179. Milesa A.J., Wallace B.A. (2006) Synchrotron radiation circular dichroism spectroscopy of proteins and applications in structural and functional genomics. Chem Soc Rev;35:39–51.
180. Thulstrup P.W., Brask J., Jensen K.J., Larsen E. (2005) Synchrotron radiation circular dichroism spectroscopy: Applied to metmyoglobin and a 4-α-helix bundle carboprotein. Biopolymers;78:46–52.
181. Gekko K., Yonehara R., Sakurada Y., Matsuo K. (2005) Structure analyses of biomolecules using a synchrotron radiation circular dichroism spectrophotometer. J Elec Spec Rel Phen;144–147: 295–297.
182. Lewis J.W., Goldbeck R.A., Kligler D.S. (1992) Time-resolved circular dichroism spectroscopy: experiment, theory, and applications to biological systems. J Phys Chem;96:5243–5254.
183. Werner E. (2007) All systems go. Nature;446:493–494.